POLITECNICO DI MILANO

Scuola di Ingegneria Industriale e dell'Informazione

Corso di Laurea Magistrale in
Ingegneria Matematica

Mathematical modelling of avascular tumor growth: travelling wave analysis and numerical simulations

Relatore: Prof. Davide AMBROSI

Correlatore: Prof. Mark CHAPLAIN

Tesi di Laurea di:

Daniele Boaretti Matr. 852555

Anno Accademico 2016 - 2017

Ringraziamenti

Con questo lavoro si conclude il mio percorso di Laurea Magistrale a Milano, contraddistinto da tanta fatica e dedizione dall'inizio alla fine. Vorrei, quindi, spendere alcune doverose parole per ringraziare le persone che mi hanno accompagnato lungo il cammino che mi ha portato fino a qui. Ringrazio tutti i miei amici, partendo da quelli di Sambe (Ferrara), passando per quelli conosciuti nel primo anno di residenza universitaria a Milano, fino ai colleghi di facoltà, perché con loro ho vissuto esperienze significative sia in ambito accademico che non. In particolare, ringrazio Lucione, Ua, Labbro, Breava, Nafti, Occiao, Enrico, Pepos, Avo, Ciccio, Kaiser, Caccia per i momenti vissuti insieme che porterò sempre nel cuore. Ringrazio l'esperienza Scout, e quindi sia i compagni che gli educatori con cui ho vissuto questo percorso, in quanto sono stati importanti per avermi formato come persona e per avermi dato tutti gli strumenti necessari a superare le avversità della vita e ad apprezzare il prossimo.

Infine ringrazio sentitamente:

PROF. DAVIDE AMBROSI per avermi dato l'opportunità di scoprire una realtà diversa da quella del Politecnico di Milano. E' stata un'occasione importante per poter conoscere un modo diverso di approcciare lo studio della materia;

PROF. MARK CHAPLAIN per avermi guidato nella scoperta del mondo della modellistica del tumore, che è molto più articolata e complessa di quanto potessi immaginare;

DR. TOMMASO LORENZI per il supporto, l'assistenza e la pazienza che mi ha sempre rivolto durante il periodo di lavoro di tesi;

LA MIA FAMIGLIA per avermi costantemente supportato, sopportato e consigliato in ogni passo importante della mia vita.

Milano, Dicembre 2017 D. B.

Alla mia famiglia.

Contents

List of Figures

List of Tables

Listings

Sommario

L'approccio comune a molti modelli matematici usati per studiare la fase avascolare dello sviluppo di un tumore solido è la descrizione del sistema mediante equazioni differenziali a derivate parziali. Lo studio di questi problemi comprende la ricerca di soluzioni di tipo onda viaggiante e la risoluzione numerica delle equazioni corrispondenti in una o più dimensioni spaziali.

Nella fase avascolare, la massa tumorale è formata da un nucleo interno di cellule necrotiche e quiescenti e da uno strato più esterno di cellule proliferanti; un buon modello matematico dovrebbe essere in grado di riprodurre questa semplice struttura. Queste osservazioni hanno ispirato il presente lavoro di tesi, il cui obiettivo è elaborare e analizzare un modello che studi la dinamica delle cellule proliferanti e quiescenti, della matrice extracellulare e dell'ossigeno in fase avascolare, rappresentando in modo biologicamente accurato fenomeni importanti, come la chemotassi e l'aptotassi. Il modello sviluppato è un sistema di quattro equazioni differenziali alle derivate parziali.

L'analisi matematica mostra che in assenza di chemotassi e aptotassi esistono due possibili forme di soluzioni di tipo onda viaggiante. Nella seconda parte della tesi vengono presentate diverse simulazioni numeriche del modello con o senza aptotassi e chemotassi, utilizzando il metodo delle differenze finite centrate in spazio e BDF in tempo.

In conclusione, questo lavoro conferma l'esistenza di soluzioni di tipo onda viaggiante in un modello tumorale nuovo semplice, che tuttavia cattura gli elementi principali del sistema, e sviluppa simulazioni numeriche per il modello completo.

Parole chiave: Evoluzione del tumore, Aptotassi, Chemotassi, Onde viaggianti, Simulazioni numeriche

Abstract

A common approach to many mathematical models of the avascular phase of solid tumour growth and dynamics is the description of the system using partial differential equations. This includes studying the existence of travelling wave solutions and developing numerical simulations in one or more spatial dimensions. At this stage of its growth, the tumour mass is composed of an inner section of necrotic and quiescent cells and an outer thin rim of proliferating cells, and a good mathematical model should be able to reproduce this basic structure. Inspired by this, the present study aims to study the dynamic of proliferating and quiescent cells, of extracellular matrix and oxygen in the avascular phase, including some important phenomena, such as chemotaxis and haptotaxis. The model reads as a system of four partial differential equations.

From the mathematical analysis carried out, we show that travelling wave solutions exist for the model without haptotaxis and chemotaxis, and there are two possible shapes of travelling waves. Furthermore, we present some numerical simulations of the model with and without haptotaxis and chemotaxis, employing the centered finite difference scheme in space and BDF in time.

To conclude, this work proposes a simple model for the tumour system, we prove the existence of travelling wave solutions in a simplified form, depicting their main properties, and we perform numerical simulations for the whole system.

Keywords: Tumour growth, Haptotaxis, Chemotaxis, Travelling wave, Numerical simulations

Chapter 1

Introduction

For over a decade there has been a growing amount of biological data concerning cancer growth and development (at many different spatial and temporal scales) that has to be analysed in a critical way. Quantitative multidisciplinary approaches have the ability to synthesize these data and bring them together in a coherent manner. Consequently, quantitative cancer models are entering the mainstream of cancer biology publications. Mathematical modelling can be useful to give scientists a deeper insight into tumour evolution as well as to predict a patient's prognosis and support optimal treatment regimens. The power of modern applied mathematics and nonlinear models is to go beyond what human intuition and linear thinking can take us.

1.1 Key aspects of biology of cancer

Most of the steps of tumour formation are nowadays understood in considerable details. In contrast, the late steps of tumour progression involve still unresolved problems of cancer pathogenesis. Tumour progression is the evolution of normal cells into cells with increasingly neoplastic phenotypes. The initialization of cancer can be tracked back from a single normal cell which, due to external factors or random mutations, undergoes a genetic modification that gives it the characteristics of a cancer cell. In particular, mutations can arise by random errors in DNA replication, by carcinogens (such as tobacco, chemicals, benzene, possibly acrylamide), by some food additives, X-rays, or ultraviolet light, by specific viruses, such as papilloma virus, or some inherited mutated genes (BRCA1 e BRCA2) [11]. According to research findings from the Cancer Genome Project, most cancer cells possess 60 or more mutations. In 2000 Douglas Hanahan and

Robert Weinberg [23] proposed a heterotypic model that defines tumours as complex tissues, according to six hallmarks:

- Immortality: Continuous cell division and limitless replication;
- Produce ‘Go’ signals (growth factors from oncogenes)
- Override ‘Stop’ signals (anti-growth signals from tumour suppressor genes);
- Resistance to cell death (apoptosis);
- Angiogenesis: Induction of new blood vessel growth;
- Metastasis: Spread to other sites.

In Figure 1.1 there is a scheme of those hallmarks.
Almost all cancer cells share some or all of the 6 traits described above, depending on the type. Some tumours may have all of these characteristics because of mutations in one key gene (e.g. the p53 gene regulates at least 4 of the traits) whereas other tumours may need more than 1 mutation for progression.

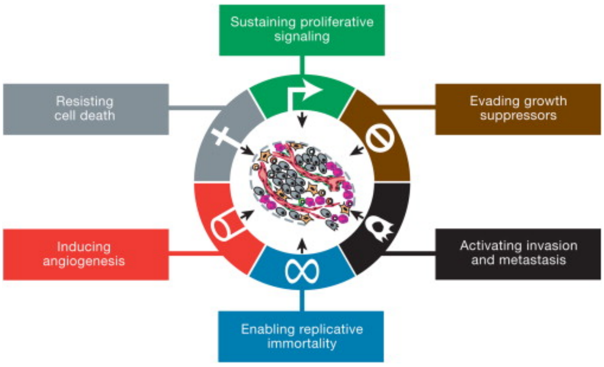

Figure 1.1: The six hallmarks of cancer identified by Hanahan and Weinberg [8]. Reprinted from: Cell, vol. 144 (5), D. Hanahan and R. A. Weinberg, "Hallmarks of Cancer: The Next Generation" pp. 646-74, Mar 2011, Copyright 2011, with permission from Elsevier.

In 2011 Hanahan and Weinberg [8] added another four hallmarks. These were defined as “emerging hallmarks” possessed by tumour cells:

- Deregulating cellular energetics;
- Avoiding immune destruction;

- Tumour-promoting inflammation;
- Genome instability and mutation.

In Figure 1.2 there is a scheme of those last hallmarks.

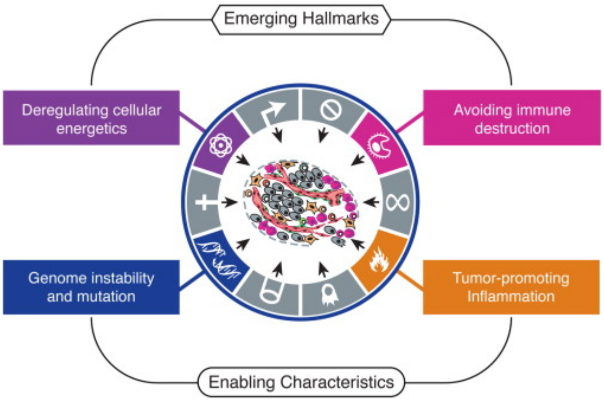

Figure 1.2: The four hallmarks of cancer identified in 2011 [8]. Reprinted from: Cell, vol. 144 (5), D. Hanahan and R. A. Weinberg, "Hallmarks of Cancer: The Next Generation" pp. 646-74, Mar 2011, Copyright 2011, with permission from Elsevier.

Using the most recent imaging techniques, it is possible to detect a tumour mass containing around 10^9 cancer cells, corresponding to a volume of a few cubic millimetres. Before we can observe it, the tumour mass is still benign. The order of magnitude leading to death is around 10^{12} cancer cells, so there is a huge gap between these two scales.

1.1.1 Aspects of solid tumour growth

The great majority (>80%) of life-threatening cancers occur in epithelial tissues, yielding carcinomas[15]. The epithelial tissues are generally made bof thin sheets of epithelial cells sitting on the top of deep, complex layers of stroma. The two layers are separated by a specialized type of extracellular matrix (ECM), known as the basement membrane (BM). This proteinaceous meshwork is constructed collaboratively by proteins secreted by both epithelial and stromal cells. It is on the epithelial side of the basement membrane that the carcinomas begin to develop and are said to be benign as long as the cells forming them remain on this side. The initial phase growth is called *in situ* and the cells have a proliferating phenotype, but not worse. These cells may entirely replace the normal

epithelial cells over considerable distances, but they do not pass the barrier of the basement membrane (BM) and invade underlying tissues; they duplicate and the tumour mass increases because of the pressure caused by the volume they have to occupy. However, the cells are still close one to the other due to adhesion forces. By definition, carcinomas born on the epithelial side of the basement membrane are said to be *benign* as long as the cells forming them remain on this side.
The cells of this solid tumour, arising from epithelial cells, can break away from the primary tumour and attach to and degrade the protein structures that make up the surrounding extracellular matrix (ECM). The cancer cells begin to invade the nearby stroma individually or in groups, so this mass of neoplastic cells is now reclassified as *malignant.*
Breaching the basement membrane is the first step in the transition from *in situ* carcinoma to invasive, potentially metastatic cancer.
The basement membrane is composed of a complex of structural proteins. Interactions of tumour cells with basement membranes and ECM components comprise two critical phases: adhesion and matrix dissolution.

Adhesion Epithelial cells are normally polarized and attached to each other via different types of cell-to-cell junctions, as well as through intercellular adhesion molecules such as E-Cadherin. Initiation of metastasis requires releasing cells from cell-to-cell contacts that keep them in their proper place in the epithelium. Thus, cancer cells usually demonstrate multiple changes in the expression of cell adhesion components. E-Cadherin, in particular, is a frequent target for genetic or epigenetic alterations that down-regulate its function, which may be considered as a tumour suppressor gene.
Epithelial cells entertain contacts with the basal membranes and with the ECM through many classes of molecules. Among them, integrins are important: changes in their expression patterns may have a profound influence on enabling cancer cells to adapt to changes in their microenvironment, a pre-requisite for a successful migration. Integrins are cell surface receptors that mediate a dual, signalling and adhesion function.
Integrins couple the ECM outside the cell to the intracellular cytoskeleton. This bond ensures that the cell can tightly adhere to ECM components without being sheared and ripped away by ECM movements. Carter has defined haptotaxis to be the movement of cells on an adhesion gradient, in the direction of increasing substrate adhesion [38], that is, in the direction of increasing density of bound integrin-ligand complexes.

Matrix dissolution One important group of enzymes is the matrix metalloproteinases (MMP). MMPs are more active in cancer cells and/or in surrounding normal stromal cells, indicating that cancer cells can somehow induce stromal cells to secrete factors that facilitate migration, invasion and, ultimately, metastasis.
MMPs have not only a direct role in degrading ECM components, but also indirectly are involved in promoting metastasis through their roles in angiogenesis. The formation of capillary sprouts is a physiological process that requires localised proteolysis of the stroma.

Metastatic dissemination Dissemination starts when aggressive tumour cells enter the bloodstream through the newly formed vasculature that they have attracted. This process is facilitated by the particular, incomplete and leaky structure of the blood vessels.
Once they have intravasated into the lumen of a blood or lymphatic vessel, individual cancer cells may travel with the blood or lymphatic fluid to other areas in the body. These long-range migrations are very dangerous. Like normal cells, the cancer cells may continue to depend on anchorage to solid substrates; without such attachment, the migrating cells may die rapidly from *anoikis* to escape recognition and destruction by the immune system and to recruit partners that facilitate their circulation and extravasation.
Disseminating cancer cells avoid immunosurveillance through two mechanisms: the outgrowth of poorly immunogenic tumour-cell variants (immunoselection) and the subversion of the immune system (immunosubversion). The first includes a series of mechanisms by which disseminating cancer cells conceal or down-regulate antigens and recognise molecular complexes at their surface. The second mechanism includes the production of sets of cytokines that down-regulate immune responses. Briefly, metastasis appears to correlate with changes in the immunogenic properties of tumour cells.

Metastatic colonisation When disseminating cancer cells leave the blood stream to enter the parenchyma of another organ the *extravasation* process begins. Metastatic cells extravasate by breaching the capillaries in which they are embedded, either by vascular-remodelling events that allow migration across the capillary wall or, as a result of mechanical disruption of capillaries, by expanding tumour emboli. In another organ, tumour cells live in a different microenvironment in which they must survive, develop, and eventually expanding the same way as they did in their organ of origin. To help them in the process of establishing a new “home” in their adoptive tissue, cancer cells recruit different cells that provide a permissive "niche" for metastasis. Once metastatic cells are established, active colonisation proceeds through the recruitment of organ-specific components of the tumour microenvironment. Full metastatic colonisation can occur by the immediate growth of cancer cells upon their extravasation, or after a prolonged period of micrometastatic dormancy.

1.2 Modelling the avascular phase

This work focuses on the mathematical modelling of avascular tumour growth, i.e., tumours without blood vessels. Avascular tumour growth is simpler to model mathematically, and yet contains many of the phenomena to be addressed in a general model of vascular tumour growth.
Nevertheless, the reproducibility of experiments with avascular tumours makes for an improved quality and increased quantity of experimental evidence that for vascular tumours, in which are often hard to isolate individual effects. In addition, experiments on vascular and metastatic tumours are much more time consuming and difficult as they have to be performed in vivo. To overcome this difficulty, avascular tumour modelling can be of use when making predictions and designing for those experiments.

1.2.1 Different regions within the tumour

When cancer cells have enough nutrient supplied by the micro-environment they proliferate, otherwise cell death (*apoptosis*) is triggered. In intermediate nutrient levels the tumour cells stay quiescent. The different of nutrient inside the tumour spheroid are determined by the diffusion and consumption of nutrients within the tumour.
During the avascular stage of growth, the tumour receives nutrient supply by diffusion from the surrounding tissue. In this phase, the tumour has not yet developed a blood supply network, therefore available nutrients are not sufficient to ensure continued exponential growth of the tumour cell mass despite the continuous nutrient supply at the tumour surface. Thus, avascular tumour undergoes a quasi-exponential growth phase followed by a saturation phase in which the volume grows linearly. The restricted supply of critical nutrients, such as oxygen and glucose, results in marked gradients within the cell mass.
A descriptive model to explain the regulation of growth and viability in spheroids, reproducing work like [32], postulates that, at early stages of development, both growth promoters and viability promoters can reach

all of the cells in the spheroid. During this early stage, the aggregate is composed of proliferating, viable cells. As the spheroid grows in size, the concentration of growth promoters decreases in the spheroid centre, which eventually falls below a critical value such that cells undergo proliferation arrest and become quiescent. Therefore, we have an inner part of quiescent cells and an outer part of living cells, which continues to proliferate. As a result, the size of tumour continues to increase, while the central concentration of viability promoters continues to decrease. Once the latter falls under a critical value, necrotic cell death occurs and the spheroids acquire a necrotic centre. This state takes place when the tumour size is $\sim 1mm$, that is around 10^6 cells, and the phenomenon is *necrosis*. These begin to die without control. Continued cellular metabolism and the process of necrosis cause both growth and viability inhibitors to be secreted and accumulate in the spheroid. As soon as the concentration of growth inhibitors reaches a critical value in the outer spheroid region, cell proliferation is further reduced. Eventually, the thickness of the proliferating layer of cells is reduced to a point at which the number of new cells is equal to the number of cells lost by cell shedding, causing saturation in the spheroid growth.

Experimental data support the idea that simple molecules involved in energy metabolism, such as oxygen and glucose, are the viability promoters in spheroids [32].

The complexity of these processes should be taken into account by a predictive model of avascular tumour growth. Important elements that need to be incorporated in such a model include cell proliferation and growth, nutrient consumption and diffusion, waste product production and diffusion, effects of growth promoting and inhibitory factors, intercellular adhesion, and cell-environment interactions, as well as the geometry of the tumour and the cells.

1.3 State-of-art of tumour modelling

Mathematical modelling is an iterative process that should not end with the first set of predictions and its success relies on continued collaboration between experimentalists and theoreticians. The earliest spatio-temporal models of avascular tumour growth describe how the size and structure of three-dimensional multicellular spheroids (MCS) change when culture conditions are manipulated [10].

In the present work, the aim is to describe some of the most widely used mathematical models in the area of avascular tumour growth. Most models of avascular tumour fall into two categories: (1) continuum mathematical models that assume the continuum assumption and thus consist of a synthesis of partial differential equations; and (2) discrete cell population models that consider processes occurring on the single cell scale and introduce cell-cell interaction using cellular automata–type computational machinery. We will discuss the main characteristics of the first approach.

1.3.1 Continuum Cell Population Models

Mathematical models describing continuum cell populations and their evolution in time classically consider the interaction between the cell mass density per unit volume and one or more chemical species that provide nutrients or influence the cell cycle events of a tumour cell population. Thus these models typically rewrite as reaction-diffusion-convection equations. A usual modelling of tumour growth in the avascular phase exploits the observation that the tumour contours sharp defined. This leads to consider geometric models where the tumour is defined as an expanding set $\Omega(t)$, which in the simplest case can be a “spheroid”. One assumes that the tumour has a constant density of mass, to account for the incompressibility of tissue. Then, the question is to describe the evolution of the dynamics of free boundary $\partial\Omega(t)$.

Model I The first free boundary problem for tumour growth dates back to H. Greenspan in 1972 [36]. He observed that in the typical steady state configuration the tumour is a sphere, a few millimetres in diameter, which histological examination shows to be made of three distinct concentric annular shells. In the thin outermost shell, a layer several cells thick, cells are observed to grow and divide as they do in the initial exponential phase. In the adjoining shell, cells are alive and viable but exhibit almost no mitosis and proliferation, so they are defined quiescent. The innermost central core consists of necrotic debris in various stages of disintegration. Greenspan proposed a radially symmetric model employing the Heaviside function for modelling the necrotic part. Figure 1.3 shows the scheme of tumoural spheroid.

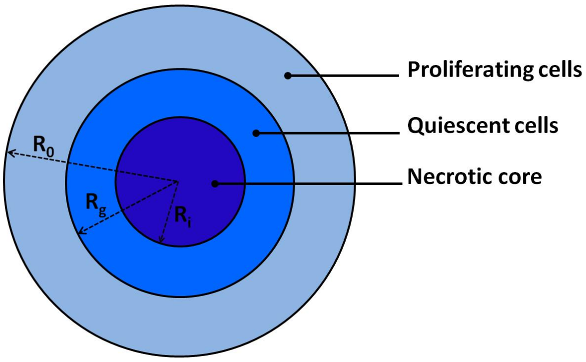

Figure 1.3: Cross-section of a nodular carcinoma showing the central necrotic core, $r \le R_i$, the layer of viable non-proliferating cells, $R_i \le r \le R_g$, and the outer shell where all mitosis occurs, $R_g \le r \le R_0$.

The avascular model considers a chemical inhibitor which is produced in the necrotic core and inhibits the mitosis of cancer cells without causing their death. The derivation of the model is obtained through conservation of mass ad reaction-diffusion equations.
Many variants have been developed in later times. It is now a well-established subject with many surveys available. In fact, this model was studied further in detail by Greenspan in 1976 [35]. In this subsequent paper, he explained the distribution of nutrients related to the growth and movement of certain cell cultures and solid tumours. He investigated the unstable development of tumours when the internal pressure forces overcome surface tension and adhesion. This later work describes the relationship between the nutrient concentration, the pressure on the surface and the surface-tension force. He states that if the tumour reaches a critical size beyond which surface tension is overcome by pressure forces, the tumour becomes unstable. It is shown that in the necrotic core, the propensity of the colony to distort by either growth or the elimination of material can reverse the effect of stability on the surface tension and, on the other hand, by controlling the distribution of nutrient, a steady state equilibrium can be reached.

In the literature, the simplest geometrical model of tumour growth is based on variation of intracellular pressure by cell division without reference to a nutrient which is supposed sufficient, so it's a purely mechanical model.

Model II The model presented now is taken from Friedman in 2004 [19]. We suppose that the density of cells is a constant ρ within the tumour that occupies the spatial domain $\Omega(t)$. The tumour still grows with the normal velocity on its boundary

$$\dot{X}(t) = v(X(t), t), \qquad X(t) \in \partial\Omega(t) \tag{1.1}$$

The growth rate $G(p)$ is related to the pressure and it satisfies the following equation:

$$\nabla \cdot v = G(p). \tag{1.2}$$

The pressure dependent growth term is supposed to satisfy for some $K > 0$,

$$G'(\cdot) < 0, \qquad G(K) = 0.$$

Then, the Darcy's assumption allows us to relate the growth speed and the pressure with

$$v(t, x) = -\nabla p(x, t) \tag{1.3}$$

Substituting (1.3) in (1.2) we obtain

$$\begin{cases} -\nabla^2 p = G(p) & x \in \Omega(t) \\ \quad p = 0 & \text{on } \partial\Omega(t). \end{cases} \tag{1.4}$$

Model III We can enrich this model as explained by Byrne and Chaplain [28], considering the tumour as a spheroid, that is a ball $B_{R(t)}$ of $\mathbb{R}^3$ centred in the origin and radius $R(t)$, and the cell population density is still constant inside this ball. The available nutrient is denoted by $c(x;t)$ for $0 \leq |x| \leq R(t)$ and is provided from the boundary $\partial B_{R(t)}$ with a concentration c_b (blood concentration). Taking into account the fact that nutrients diffuse and degrade in time [25], the system reads

$$\begin{cases} \partial_t c - \nabla^2 c + \lambda c = 0 & x \in B_{R(t)} \\ \qquad c = c_b & \text{on } \partial B_{R(t)} \end{cases} \tag{1.5}$$

with the equation for $R(t)$ found by integration of (1.2)

$$\dot{R}(t) = \frac{1}{R^2} \int_0^{R(t)} G(c)\, r^2\, dr, \qquad R(0) = R^0 > 0 \tag{1.6}$$

In the equation on c the nutrient is consumed with rate λ. The function $G : [0, c_b] \to \mathbb{R}$ determines the net growth rate of cells, depending upon the available nutrient. We make the general assumption on $G \in C^1$ that there is $\bar{c} > 0$ such that it holds

$$G'(\cdot) > 0, \qquad G(\bar{c}) = 0. \tag{1.7}$$

Model IV We can combine the latter two models in the following: a pressure field equation is defined in the domain $\Omega(t)$

$$\begin{cases} -\nabla^2 p = G(c(x,t)) & x \in \Omega(t) \\ \quad p = 0 & \text{on } \partial\Omega(t) \end{cases} \tag{1.8}$$

with the equation for nutrient (1.5); the domain moves with velocity $-\nabla p(x,t) \cdot \mathbf{n}$, $\mathbf{n}$ being the outward unit normal to the boundary $\Omega(t)$:

$$\dot{X}(t) = -\nabla p(X(t), t) \cdot \mathbf{n}(X(t), t)$$

Model V This geometric description can be extended to include more biological ingredients in the model, as quiescent cells. A first simple approach is to ignore the nutrients and introduce cell densities $n_P(x;t)$, $n_Q(x;t)$ and $n_D(x;t)$ for proliferating, quiescent and dead cells. We recall from the experimental observations most of the cells are in a quiescent state and only a small amount is in proliferative state. Transitions between these two states are controlled by various environmental conditions as nutrients, space availability, TGF (Tumor Growth Factors). Following the steps adopted by Friedman in 2004 [19], the cell movement of several species is included as

$$\begin{cases} \partial_t n_P + \nabla \cdot (v n_P) = G(n_P, n_Q) - a n_P + b n_Q & x \in \Omega(t), \\ \partial_t n_Q + \nabla \cdot (v n_Q) = a n_p - b n_Q - d n_Q, \\ \partial_t n_D + \nabla \cdot (v n_D) = d n_Q - \mu n_D. \end{cases} \tag{1.9}$$

This is coupled with the Darcy law for velocity

$$v(x,t) = -\nabla p(x,t),$$

and the pressure enforces the incompressibility condition

$$n_P + n_Q + n_D = n_{max}, \quad \forall x \in \Omega(t), \, t \geq 0.$$

Again, the Darcy assumption provides the velocity fields:

$$-\nabla^2 p = \nabla \cdot v = G(n_P, n_Q) - \mu n_D$$

which we supplement with Dirichlet homogeneous boundary conditions:

$$p(x,t) = 0 \quad \text{for } x \in \partial\Omega(t)$$

The free boundary $\partial\Omega(t)$ moves with normal velocity $-\nabla p$

$$\dot{X}(t) = -\nabla p(X(t), t)$$

and this makes that there is no need of boundary conditions for the hyperbolic equations in (1.9).

Model VI We present an example of a mathematical diffusive model for avascular tumour growth, explained by Anderson, Chaplain et al. in 2000 [24]. For sake of simplicity, we assume that the tumour solid mass is in the avascular phase, so that cells receive oxygen only through diffusion. In the model four time and space dependent variables are taken into account: the tumour cells density n, the extracellular matrix degrading enzymes (MDEs) m, the extracellular matrix density f and tumour angiogenic factors (TAF) c. As well as making space into which tumour cells may move by simple diffusion (random motility), we assume that this' also results in a gradient of these bound cell-adhesion molecules, such as fibronectin. By definition, haptotaxis is the directed migratory response of cells to gradients of fixed or bound chemicals. a response to gradients of bound macromolecules such as fibronectin. To incorporate this phenomenon in this model, we define

$$\mathbf{v}_{hapto} := \chi \nabla f, \tag{1.10}$$

thus we take the haptotactic flux to be:

$$\mathbf{J}_{hapto} = n\mathbf{v}_{hapto} = \chi\, n \nabla f, \tag{1.11}$$

where χ is the (constant) haptotactic coefficient. To describe the random motility of the tumour cells we assume a flux of the form

$$\mathbf{J}_{random} = -D\left(f, m\right) \nabla n, \tag{1.12}$$

where $D\left(f, m\right)$ may be a constant or a function of either the MDE or ECM concentration. Focussing entirely on the cell-matrix interactions and how these interactions affect tumour cell migration, we do not consider any proliferation of tumour cells in the partial differential equation model. The conservation equation for the tumour cell density n is therefore given by

$$\frac{\partial n}{\partial t} + \nabla \cdot \left(\mathbf{J}_{random} + \mathbf{J}_{hapto}\right) = 0,$$

and hence the partial differential equation governing tumour cell motion (in the absence of cell proliferation) is

$$\frac{\partial n}{\partial t} = \nabla \cdot \left(D\left(f, m\right) \nabla n\right) - \chi \nabla \cdot \left(n \nabla f\right). \tag{1.13}$$

We assume that the MDEs degrade ECM upon contact and hence the degradation process is modelled by the following simple equation:

$$\frac{\partial f}{\partial t} = -\delta\, f\, m, \tag{1.14}$$

where δ is a positive constant.
Active MDEs are produced by the tumour cells, diffuse throughout the tissue and undergo some form of decay. The equation governing the evolution of MDE concentration is therefore given by

$$\frac{\partial m}{\partial t} = D_m \nabla^2 m + g(n,m) - h(n,m,f) \tag{1.15}$$

where D_m is a positive constant, the MDE diffusion coefficient, g is a function modelling the production of active MDEs by tumour cells and h is a function modelling the MDE decay.

The existence of travelling wave solutions and patterns for the model under study has been addressed in several works, see [5]. Travelling wave solutions are of particular interest from the biological point as the diameter of 2D monolayers, 3D multicellular spheroids and Xenografts, 3D tumours emerging from cells injected into animals is found to increase for many cell lines linearly in time, thus indicating a constant growth speed of the tumour border [12].

Model VII In 2013 Tang et al. in [5] considered an aggregate of tumour cells as an elastic fluid. Denoting by T and $\mathbb{I}$ the Cauchy stress tensor and the identity tensor respectively, the following constitutive relation holds: $T = -p(\rho)\,\mathbb{I}$. In addition, denoting by v the velocity field and by ρ the cell population density, we will make use of the following advection-diffusion model

$$\partial_t \rho + \nabla \cdot (\rho v) - \nabla \cdot (\varepsilon \nabla \rho) = \Phi(\rho, \Sigma)$$

In this equation, the third term in the left hand side describes the random motility of cells with a nonnegative diffusion coefficient ε. The right hand side $\Phi(\rho,\Sigma)$ is the growth term; it expresses that cells divide freely, thus resulting in an exponential growth, as long as the elastic pressure Σ is less than a threshold pressure denoted by C_p where the cell division is stopped by contact inhibition (the term "homoeostatic pressure" has been used for C_p). This critical threshold is determined by the compression that a cell can experience [14]. The balance of forces acting on the cells lead, under certain hypotheses, to the following relationship between the velocity field v and the elastic pressure

$$-C_S \nabla \Sigma(\rho) = -C_z \nabla^2 v + v$$

This is Darcy's law which describes the tendency of cells to move down pressure gradients, extended to a Brinkman model by a dissipative force density resulting from internal cell friction due to cell volume changes. C_S and C_z are parameters relating respectively the reference elastic and bulk viscosity cell properties with the friction coefficient. The resulting model is then the coupling of this elliptic equation for the velocity field, a conservation equation for the population density of cells and a state equation for the pressure law.

Besides the study of the factors on avascular tumour growth, like the availability of nutrients such as glucose and oxygen, the work of Ambrosi and Mollica [20] analysed what is the role of the stress on the process of mitosis and apoptosis of tumour cells. As the role of mechanical stress in the growth of a multicell spheroid is also not negligible, and this fact is demonstrated by recent experimental results, Ambrosi and Mollica developed a mathematical model able to account for the volumetric growth of soft tissue and they applied it to the specific problem of the growth of a multicell spheroid, subjected to two growth conditions: free-suspension and gel-embedded. Their model is able to reproduce the experimental data with a satisfying qualitative agreement.

Ambrosi and Preziosi in [21] introduced a multiphase mechanical framework as a background for the deduction of tumour growth models. Their work is based on the main idea that multicell spheroids can be modelled as ensembles of deformable balloons in contact, the extracellular space being filled by the organic liquid and, in a more refined description, by the extracellular matrix. A general theoretical framework was introduced leading to a triphasic description including the extracellular matrix.

Objective of the Thesis

The main objective of this thesis is to work out formulate a model which aims to study the dynamics of proliferating and quiescent cells, interacting with the extracellular matrix and oxygen levels in the avascular phase, including some important phenomena in avascular tumour growth, like chemotaxis and haptotaxis. To do so, we will develop a model consisting of a system of partial differential equations which can be studied analytically and numerically, thus enabling the investigation of solutions of this formulation.

Outline

After the introduction, where we analysed the history of mathematical models of tumour growth, the thesis is structured as follows:

In the second chapter we introduce the mathematical model of partial differential equations and its non-dimensionalisation, using data from the literature, when available;

In the third chapter we identify the stationary states of the system and then we analyse the existence and characterisation of travelling wave solutions;

In the fourth chapter we present the numerical solutions of the system of equations in one dimension. In particular, we study the system in the presence and absence of haptotaxis and chemotaxis. Finally, we vary some key parameters to see how the solution is affected by them.

Chapter 2

The Mathematical model

The model we are going to introduce aims to characterize the avascular phase of the tumour. We consider the dynamics of the tumour cells, which we distinguish between proliferating and quiescent, and the dynamics of the extracellular tissue and the nutrient, for example oxygen. In our model, we include also haptotaxis and chemotaxis, which has been a popular phenomenon for mathematical modelling since the work of Keller and Segel [37]. Models of chemotaxis are the basis for mathematical models of cells populations that undergo haptotactic migration. These chemotaxis models usually account for the chemotactic migration of cells using a cell flux proportional to the gradient in concentration of some chemical species that is considered to be an attractant for the cells under study. On the other hand, Maini [31] developed a mechanochemical model of cell-haptotaxis to investigate the generation of one-dimensional spatial and spatio-temporal patterns. Maini's model was used to investigate the changes in the cell and ECM density and the displacement of a material point of matrix due to haptotactic migration of cells. He modelled this migration introducing the haptotactic cell flux, proportional to the gradient of the extracellular matrix density.

In this way, the model we are going to introduce is quite new with respect to the previous overview of mathematical models, because they focused only in the dynamics of different populations of cells within the tumour or the interaction of the cells one with the surrounding tissue and the nutrient availability, while this model aims to describe all these dynamics in a simple manner. The description of the dynamics of the proliferating and quiescent cells is similar to Model V [19] and Model VI [24], the former for the transition between the proliferating and quiescent states, the latter for the dynamics of ECM.

We denote by p, q, m, n the concentration of invading proliferating cells,

invading quiescent cells, the density of the extracellular matrix, the concentration of the oxygen, respectively. We take into account oxygen production from the ECM, uptake, decay [6], and we introduce the parameter γ, which is the fraction of oxygen uptake by proliferating cells. The oxygen production, uptake, and decay rate are β, $\gamma\, K_B\,(N)$, ζ, respectively.
We model the ECM with a time-dependent equation, including the degradation, by proliferating tumour cells, and remodelling of ECM by the cells present in the tissue ([9], [2]). In particular, the normal tissue is assumed to have logistic growth in order to attain its healthy state in the absence of cancer cells. Moreover, looking to previous works as [9], we omit any diffusion or transport term since the ECM does not diffuse, while we add a term of logistic growth, accordingly to [2]. The carrying capacity for the extracellular matrix is represented by k_m, while the intrinsic growth rate is η. The degradation rate by proliferating cells is denoted by α.
We model the motion of the proliferating cells including haptotaxis and chemotaxis; ρ and χ are, respectively, the haptotactic and chemotactic coefficient. The tendency of cells to move down pressure gradients is also modelled relying on the definition of the cell velocity fields through Darcy's law, which provides the following definition:

$$\Pi := K_\mu\,(p+q)^\mu\,, \tag{2.1}$$

k_p being the equilibrium value of the local cell density p, q in the presence of high oxygen concentrations, K_μ being a non-dimensional coefficient with

$$K_\mu \to 1 \quad \text{as } \mu \to \infty.$$

Moreover, we model the transition from proliferating into quiescent and vice-versa [19] with functions depending on the nutrient availability, $K_{PQ}\,(n)$ and $K_{QP}\,(n)$, respectively. We assume that proliferating cells divide at a rate that is limited by crowding effects of the total cell population, and its growth depends also on the nutrients. We model this latter dependence by $K_B\,(n)$. The functions denoting the rates introduced before have to satisfy the following hypothesis:

$$K_B\,(\cdot) \geq 0, \quad K_B'\,(\cdot) > 0, \tag{2.2}$$

$$K_{PQ}\,(n) = K\,(n)\,, \quad K_{QP}\,(n) = \varepsilon - K\,(n)\,, \tag{2.3}$$

$$\varepsilon \geq K\,(\cdot) \geq 0, \quad K'\,(\cdot) \leq 0, \tag{2.4}$$

with $\varepsilon > 0$ a constant coefficient. In addition, $K\,(n)$ should be a smooth function; a possible example could be

$$K\,(n) = \varepsilon\frac{1}{2}\,(1 - \tanh\,(a\,n - b)) + \frac{1}{2}, \quad a > 0.$$

In this way, we want to model the fact that we could have in principle both transition of the state of the cells from the proliferating to the quiescent state and vice-versa. Another possibility could be

$$K\left(n\right) = \varepsilon H\left(n_k - n\right)$$

where H is the Heaviside function, i.e., $H\left(n\right) = 1$ for $n > 0$ and $H\left(n\right) = 0$ for $n < 0$. With an appropriate choice of the parameters a and b it is possible to approximate the Heaviside function with the hyperbolic tangent function: $n_k = b/a$, $a >> 0$.
We indicate with ∇^2 with Laplacian operator, while with ∂_t the temporal derivative. The system of the equations that governs the dynamics is:

$$\begin{cases} \partial_t p + \nabla \cdot \left(\mathbf{v}_P\, p\right) = \left[K_B\left(n\right)\left(1 - \dfrac{p+q}{k_p}\right) - K_{PQ}\left(n\right)\right] p \\ \qquad\qquad + K_{QP}\left(n\right)\, q - \rho\nabla\cdot\left(p\nabla m\right) - \chi\nabla\cdot\left(p\nabla n\right) \\ \partial_t q + \nabla \cdot \left(\mathbf{v}_Q\, q\right) = K_{PQ}\left(n\right)\, p - K_{QP}\left(n\right)\, q \\ \partial_t m = -\alpha\, p\, m + \eta m\left(1 - \dfrac{m}{k_m}\right) \\ \partial_t n - D_N \nabla^2\left(n\right) = \beta\, m - \gamma\, K_B\left(n\right)\, p - \zeta\, n \end{cases} \tag{2.5}$$

where we define

$$\begin{cases} \nu_P := \dfrac{D_P}{k_p^{\mu}} \\ \nu_Q := \dfrac{D_Q}{k_p^{\mu}} \\ \mathbf{v}_P := -\nu_P \nabla\Pi\left(p,q\right) \\ \mathbf{v}_Q := -\nu_Q \nabla\Pi\left(p,q\right) \end{cases} \tag{2.6}$$

In the first equation in (2.5), the terms $K_B(n)p\left(1 - \frac{p+q}{k_p}\right)$, $-K_{PQ}(n)p$, $K_{QP}(n)p$, $-\rho\nabla\cdot(p\nabla m)$ and $-\nabla\cdot(p\nabla n)$ are proliferation, transition from proliferating to quiescent state, transition from quiescent to proliferating state, haptotaxis and chemotaxis, respectively.
In the second equation in (2.5), the terms $K_{PQ}(n)p$, $-K_{QP}(n)p$, are transition from proliferating to quiescent state and transition from quiescent to proliferating state, respectively.
In the third equation in (2.5), the terms $-\alpha\, p\, m$ and $\eta m\left(1 - \frac{m}{k_m}\right)$ are degradation from proliferating cells and logistic growth, respectively.
In the fourth equation in (2.5), the terms $-D_N\nabla^2$, $-\gamma\, K_B\left(n\right)\, p$ and $-\zeta\, n$ are production form ECM, degradation form proliferating cells and decay,

respectively.
We will assume the random motility coefficients D_P, D_Q constants. Hypothesis on coefficients: we suppose that

$$\beta k_m \geq \zeta n_k \tag{2.7}$$

2.1 Non-dimensionalization of the model

Denoting dimensionless variables by carets, we adopt the following rescalings:

$$\begin{gathered}
\hat{t} = \frac{t}{t_0}, \quad \hat{\mathbf{x}} = \frac{\mathbf{x}}{x_0} \\
\hat{p}\left(\hat{t}, \hat{\mathbf{x}}\right) = \frac{p\left(t, \mathbf{x}\right)}{k_p}, \quad \hat{q}\left(\hat{t}, \hat{\mathbf{x}}\right) = \frac{q\left(t, \mathbf{x}\right)}{k_p}, \quad \hat{m}\left(\hat{t}, \hat{\mathbf{x}}\right) = \frac{m\left(t, \mathbf{x}\right)}{k_m}, \\
\hat{n}\left(\hat{t}, \hat{\mathbf{x}}\right) = \frac{n\left(t, \mathbf{x}\right)}{n_0}, \quad \hat{\Pi} = K_\mu \left(\hat{p} + \hat{q}\right)^\mu, \quad \hat{K}_B\left(\hat{n}\right) = t_0\, K_B\left(\hat{n}\, n_0\right), \\
\hat{K}_{PQ}\left(\hat{n}\right) = t_0\, K_{PQ}\left(\hat{n} n_0\right), \quad \hat{K}_{QP}\left(\hat{n}\right) = t_0\, K_{QP}\left(\hat{n}\, n_0\right), \\
\hat{D}_N = \frac{D_N\, t_0}{x_0^2}, \quad \hat{\rho} = \frac{\rho\, t_0\, k_m}{x_0^2}, \quad \hat{\nu}_P\left(\hat{p}, \hat{q}\right) = \frac{D_P\, t_0}{x_0^2}, \\
\hat{\nu}_Q\left(\hat{p}, \hat{q}\right) = \frac{D_Q\, t_0}{x_0^2}, \quad \hat{\alpha} = \alpha\, t_0\, k_p, \quad \hat{\eta} = \eta\, t_0\, k_m, \\
\hat{\beta} = \frac{t_0\, \beta\, k_m}{n_0}, \quad \hat{\gamma} = \frac{\gamma\, k_p}{n_0}, \quad \hat{\zeta} = \zeta\, t_0, \quad \hat{\chi} = \frac{\chi\, t_0\, n_0}{x_0^2}.
\end{gathered}$$

In the Table 2.1 there are all the parameters used for the non-dimensionalization of the problem. The state in the non-dimensional form reads:

$$\begin{cases}
\partial_{\hat{t}}\hat{p} + \nabla_{\hat{\mathbf{x}}} \cdot \left(\hat{\mathbf{v}}_P\, \hat{p}\right) = \left[\hat{K}_B\left(\hat{n}\right)\left(1 - \dfrac{\hat{p} + \hat{q}}{\hat{k}_p}\right) - \hat{K}_{PQ}\left(\hat{n}\right)\right]\hat{p} \\
\qquad\qquad + \tilde{K}_{QP}\left(\hat{n}\right)\, \hat{q} - \hat{\rho}\nabla_{\hat{\mathbf{x}}} \cdot \left(\hat{p}\nabla_{\hat{\mathbf{x}}}\hat{m}\right) \\
\qquad\qquad - \hat{\chi}\nabla_{\hat{\mathbf{x}}} \cdot \left(\hat{p}\nabla_{\hat{\mathbf{x}}}\hat{n}\right) \\
\partial_{\hat{t}}\hat{q} + \nabla_{\hat{\mathbf{x}}} \cdot \left(\hat{\mathbf{v}}_Q\, \hat{q}\right) = \tilde{K}_{PQ}\left(\hat{n}\right)\, \hat{p} - \hat{K}_{QP}\left(\hat{n}\right)\, \hat{q} \\
\partial_{\hat{t}}\hat{m} = -\hat{\alpha}\, \hat{p}\, \hat{m} + \hat{\eta}\hat{m}\left(1 - \dfrac{\hat{m}}{\hat{k}_m}\right) \\
\partial_{\hat{t}}\hat{n} - \hat{D}_N\nabla^2_{\hat{\mathbf{x}}}\left(\hat{n}\right) = \hat{\beta}\, \hat{m} - \hat{\gamma}\, \hat{K}_B\left(\hat{n}\right)\, \hat{p}\, - \hat{\zeta}\, \hat{n}
\end{cases} \tag{2.8}$$

where we define

$$\begin{cases}
\hat{\mathbf{v}}_P := -\hat{\nu}_P\nabla_{\hat{\mathbf{x}}}\hat{\Pi}\left(\hat{p}, \hat{q}\right) \\
\hat{\mathbf{v}}_Q := -\hat{\nu}_Q\nabla_{\hat{\mathbf{x}}}\hat{\Pi}\left(\hat{p}, \hat{q}\right)
\end{cases} \tag{2.9}$$

The symbol $\nabla_{\hat{\mathbf{x}}}\cdot$, $\nabla_{\hat{\mathbf{x}}}$ and $\nabla^2_{\hat{\mathbf{x}}}$ stand, respectively, for the divergence, the gradient, and the Laplacian operators with respect to $\hat{\mathbf{x}}$.

Table 2.1: Parameters values used to perform numerical simulations; Assum., Dim., Non.dim. and M.M stand for assumed, dimensional, non-dimensional, Michaelis-Menten respectively

Symbol	**Meaning**	**Dim.**	**Non-dim.**	**Source**
x_0	Typical length scale of tumour	2 mm		[1] (end of avascular phase)
t_0	Typical time scale of tumour	50 days		[22] (end of avascular phase)
n_0	Reference value of oxygen	5×10^{-2} mM		[7]
k_p	Reference value of cells	1.25×10^6 cells cm^{-3}		[22]
k_m	Reference value of ECM	10^{-10} M		[34]
ρ	Haptotactic coefficient		0.05	Assum.
χ	Chemotactic coefficient		0.05	Assum.
η	ECM regenerating rate		$0.15 - 10$	[17], [16], [3]
D_P	Diffusion coefficient of proliferating cells	10^{-9} cm^2 s^{-1}	0.0014	[18] (in case of constant diffusion)

Continued on next page

Table 2.1 – *Continued from previous page*

Symbol	Meaning	Dim.	Non-dim.	Source
D_Q	Diffusion coefficient of proliferating cells	2×10^{-9} cm^2 s^{-1}	0.0028	[4](in case of constant diffusion)
D_N	Diffusion coefficient for oxygen	2×10^{-5} cm^2 s^{-1}	2.16×10^3	[33]
α	ECM consumption rate		10	[13]
β	Oxygen regeneration rate		1.296×10^6	Assum.
γ	Fraction of oxygen uptake	6.25×10^{-17} mmol cell^{-1}	3.9062×10^{-6}	[27]
ζ	Decay rate of oxygen		6.48×10^5	Assum.
v_{max}	Maximum rate of oxygen uptake	1×10^{-5} s^{-1}	43.2	[29], [27]
c_m	M.M. constant of oxygen uptake	1.83×10^{-6} M	0.2344	[29], [27]

K_B should satisfy 2.2. The first, simplest, choice is to adopt a linear function. However, this is not really correct from a biological view point since it is well-known that there is a threshold for the uptake rate of nutrients upon the cells. Therefore, we should change this function into, for example, a Michaelis-Menten type, i.e.:

$$\hat{v}_{max} = v_{max}\, t_0, \quad \hat{c}_m = \frac{c_m}{n_0}, \quad \hat{K}_B\left(\hat{n}\right) = \hat{v}_{max} \frac{\hat{n}}{\hat{c}_m + \hat{n}}.$$

In particular, c_m is the Michaelis-Menten constant which shows the concentration of the nutrient when the oxygen rate uptake is equal to one half of the maximal rate of consumption, which we denote with v_{max}. The parameters v_{max}, c_m have been chosen in agreement with the consideration made by [27] and the experimental results reported by [29].

Moreover, since some parameters are difficult to obtain because of the non-availability of experiments that can track specific phenomena, we choose some non-dimensional values which had been adopted in other works, like β, ζ, α, η, χ, ρ. All the other values will be specified in the section of the numerical analysis accordingly to the cases.

Chapter 3

Mathematical analysis

In this chapter we will go through the analysis of the mathematical model. First, we begin looking for relations to be satisfied under equilibrium. These lead us to choose the appropriate boundary conditions to adopt in the next section dedicated to the research for travelling wave solutions for the model without haptotaxis and chemotaxis. We make this choice because the flux terms related to these phenomena make the analysis more difficult. We will adopt some hypothesis on the functions to look for and, after observations, we will subdivide the analysis in two regions.

3.1 Preliminary considerations

In this section we will explore what are the relations that have to be satisfied under equilibrium. In this framework, we introduce the following K function:

$$K\left(n\right) = \varepsilon H\left(n_k - n\right)$$

where H is the Heaviside function, i.e., $H\left(n\right) = 1$ for $n > 0$ and $H\left(n\right) = 0$ for $n < 0$, and $\varepsilon > 0$ a constant coefficient. This choice satisfies the conditions (2.2). We take

$$K_{PQ}\left(n\right) = K\left(n\right), \quad K_{QP}\left(n\right) = \varepsilon - K\left(n\right). \tag{3.1}$$

In Figure 3.1 there are the plots of K_{PQ} and K_{QP} functions.

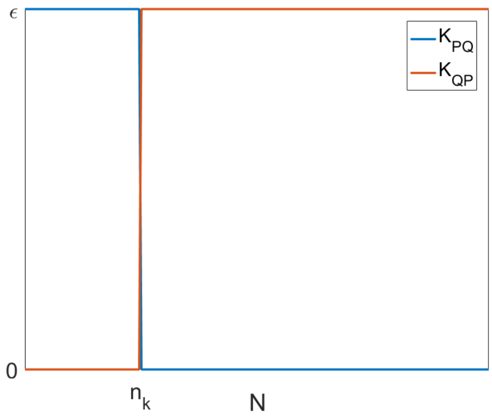

Figure 3.1: Plots of $K_{PQ}(N)$ and $K_{QP}(N)$ functions.

We can rewrite the system ((2.5)-(2.6)) under the assumption of stationary conditions as follows:

$$\begin{cases} 0 = \left[K_B\left(\bar{n}\right)\left(1-\dfrac{\bar{p}+\bar{q}}{k_p}\right) - K_{PQ}\left(\bar{n}\right)\right]\bar{p} + K_{QP}\left(\bar{n}\right)\,\bar{q} \\ 0 = K_{PQ}\left(\bar{n}\right)\,\bar{p} - K_{QP}\left(\bar{n}\right)\,\bar{q} \\ 0 = -\alpha\,\bar{p}\,\bar{m} + \eta\bar{m}\left(1-\dfrac{\bar{m}}{k_m}\right) \\ 0 = \beta\,\bar{m} - \gamma\,K_B\left(\bar{n}\right)\,\bar{p}\, - \zeta\,\bar{n} \end{cases} \tag{3.2}$$

3.1.1 Inside the tumour

First, we look for stationary states such that $\bar{n} < n_k$, which is, in a biological perspective, inside the tumour. Thus, the system (3.2) rewrites:

$$\begin{cases} 0 = \left[K_B\left(\bar{n}\right)\left(1-\dfrac{\bar{p}+\bar{q}}{k_p}\right) - \varepsilon\right]\bar{p} \\ 0 = \varepsilon\,\bar{p} \\ 0 = -\alpha\,\bar{p}\,\bar{m} + \eta\bar{m}\left(1-\dfrac{\bar{m}}{k_m}\right) \\ 0 = \beta\,\bar{m} - \gamma\,K_B\left(\bar{n}\right)\,\bar{p}\, - \zeta\,\bar{n} \end{cases} \tag{3.3}$$

As a result, from the second equation we deduce that $\bar{p} = 0$. Therefore, the value $\bar{q}$ is not determined. From the last equation we deduce that

$$\bar{n} = \frac{\beta}{\zeta}\bar{m} < n_k. \tag{3.4}$$

Moreover, the third equation leads to

$$0 = \eta\,\bar{m}\left(1 - \frac{\bar{m}}{k_m}\right). \tag{3.5}$$

As a result, we obtain

$$\bar{m} = 0 \vee \bar{m} = k_m. \tag{3.6}$$

Inside the tumour we expect that the ECM is not at the reference value k_m, so we have

$$\bar{m} = 0, \quad \bar{n} = 0 \quad \text{from (3.4)}. \tag{3.7}$$

The value of $\bar{q}$ is still not determined. We choose $\bar{q} = k_p$. To sum up, we have obtained

$$\bar{p} = 0, \quad \bar{q} = k_p, \quad \bar{m} = 0, \quad \bar{n} = 0. \tag{3.8}$$

3.1.2 Outside the tumour

We look for stationary states such that $\bar{n} \geq n_k$, which is, in a biological perspective, outside the tumour. Thus, the system becomes:

$$\begin{cases} 0 = \left[K_B\left(\bar{n}\right)\left(1 - \dfrac{\bar{p}+\bar{q}}{k_p}\right)\right]\bar{p} + \varepsilon\,\bar{q} \\ 0 = -\varepsilon\,\bar{q} \\ 0 = -\alpha\,\bar{p}\,\bar{m} + \eta\bar{m}\left(1 - \dfrac{\bar{m}}{k_m}\right) \\ 0 = \beta\,\bar{m} - \gamma\,K_B\left(\bar{n}\right)\,\bar{p}\, - \zeta\,\bar{n} \end{cases} \tag{3.9}$$

As a result, from the second equation we deduce that $\bar{q} = 0$. The first equation simplifies in

$$0 = \left[K_B\left(\bar{n}\right)\left(1 - \frac{\bar{p}}{k_p}\right)\right]\bar{p}. \tag{3.10}$$

Since we are outside the tumour, we discard $\bar{n} = 0, \vee \bar{p} = k_p$ and we choose the biological solution is $\bar{p} = 0$. Moreover, the third equation leads to

$$0 = \eta\,\bar{m}\left(1 - \frac{\bar{m}}{k_m}\right). \tag{3.11}$$

There are two possible solutions: $\bar{m} = 0, \bar{m} = k_m$. If $\bar{m} = 0$, then from the fourth equation we have $\bar{n} = 0$, which is incompatible with the condition we adopted at the beginning of this subsection $\bar{n} > n_k > 0$. As a result, we have

$$\bar{m} = 0, \quad \bar{n} = \frac{\beta}{\zeta} k_m > n_k. \tag{3.12}$$

From the last equation we deduce that

$$\bar{n} = \frac{\beta}{\zeta} \bar{m} \geq n_k. \tag{3.13}$$

Therefore, if we suppose that $\bar{m} = 0$, we can't satisfy the condition assumed in this subsection $\bar{n} \geq n_k > 0$, so we discard the solution $\bar{m} = 0$. As a result, we obtain:

$$\bar{p} = 0, \quad \bar{q} = 0, \quad \bar{m} = k_m, \quad \bar{n} = \frac{\beta}{\zeta} k_m. \tag{3.14}$$

Having in mind the hypothesis on the coefficients (2.7), these equilibria exist and make biologically sense, because in this subsection we are outside the tumour and the nutrient concentration and ECM are not affected in the avascular phase of tumour growth.

3.2 Travelling wave solutions

We want to construct travelling wave solutions of the form $p\left(x,t\right) = P\left(z\right)$, $q\left(x,t\right) = Q\left(z\right)$, $m\left(x,t\right) = M\left(z\right)$, $n\left(x,t\right) = N\left(z\right)$, $z = x - at$, where $a > 0$ is the wave speed. Substituting these ansatzs forms into (2.5) gives the ODEs:

$$\begin{cases} -aP' - \left[P\,\nu_P \Pi'\right]' = \Bigg[K_B\left(N\right)\left(1 - \dfrac{P+Q}{k_p}\right) \\ \qquad\qquad\qquad -K_{PQ}\left(N\right)\Bigg] P + K_{QP}\left(N\right) Q \\ \qquad\qquad\qquad - \rho\left(PM'\right)' - \chi\left(PN'\right)' \\ -aQ' - \left[Q\,\nu_Q \Pi'\right]' = K_{PQ}\left(N\right)\,P - K_{QP}\left(N\right)\,Q \\ \qquad\qquad -aM' = -\alpha P\,M + \eta M\left(1 - \dfrac{M}{k_m}\right) \\ \quad -aN' - D_N N'' = \beta\,M - \gamma\,K_B\left(N\right)\,P - \zeta\,N \end{cases} \tag{3.15}$$

We put $\rho = \chi = 0$. The system to analyse is the following:

$$\begin{cases} -aP' - \left[P\,\nu_P \Pi'\right]' = \left[K_B\left(N\right)\left(1 - \dfrac{P+Q}{k_p}\right)\right. \\ \qquad\qquad\qquad\qquad \left. -K_{PQ}\left(N\right)\right]P + K_{QP}\left(N\right)Q \\ -aQ' - \left[Q\,\nu_Q \Pi'\right]' = K_{PQ}\left(N\right)\,P - K_{QP}\left(N\right)\,Q \\ \qquad\qquad -aM' = -\alpha P\,M + \eta M\left(1 - \dfrac{M}{k_m}\right) \\ \quad -aN' - D_N N'' = \beta\,M - \gamma\,K_B\left(N\right)\,P - \zeta\,N \end{cases} \tag{3.16}$$

We note that the third equation in (3.16) is an equation where the independent variable is $z = t$ and x is a parameter which is present only through P. Therefore, we construct travelling wave solutions of the form $p\left(x,t\right) = P\left(z\right)$, $q\left(x,t\right) = Q\left(z\right)$, $m\left(x,t\right) = M\left(t;x\right)$, $n\left(x,t\right) = N\left(z\right)$, $z = x - at$, where $a > 0$ is the wave speed.
We search for solutions that satisfy the following properties:

$$\mathrm{Supp}(Q) \subseteq (-\infty, 0], \quad P(+\infty) = 0, \tag{3.17}$$

$$P\left(-\infty\right) = 0, \quad Q\left(-\infty\right) = k_p, \tag{3.18}$$

$$P\left(0\right) = k_p, \quad Q\left(0\right) = 0, \tag{3.19}$$

$$M(0;x) = k_m \quad \text{(initial condition for M)} \tag{3.20}$$

$$N\left(-\infty\right) = 0, \quad N\left(+\infty\right) = \frac{\beta}{\zeta}k_m > n_k \tag{3.21}$$

In this framework, we introduce the following K function:

$$K\left(n\right) = \varepsilon H\left(n_k - n\right)$$

where H is the Heaviside function, i.e., $H\left(n\right) = 1$ for $n > 0$ and $H\left(n\right) = 0$ for $n < 0$, and $\varepsilon > 0$ a constant coefficient. This choice satisfy the conditions (2.2). We take

$$K_{PQ}\left(n\right) = K\left(n\right), \quad K_{QP}\left(n\right) = \varepsilon - K\left(n\right). \tag{3.22}$$

3.2.1 M equation

First of all, let's consider the third equation in (3.16). It can be rewritten as follows:

$$aM' = \eta\left[\frac{M}{k_m} - \left(1 - \frac{\alpha\,P}{\eta}\right)\right]M. \tag{3.23}$$

For a given x, if we suppose that M attains a maximum greater than k_m in t^*, then $M'(t^*;x) = 0$, $M(t^*;x) = M^* > k_m > 0$, and

$$0 = -\alpha\, PM^* + \eta\, M^* \left(1 - \frac{M^*}{k_m}\right).$$

Simplifying the equation gives

$$P = \frac{\eta}{\alpha}\left(1 - \frac{M^*}{k_m}\right) < 0$$

which does not make biologically sense.This argument is valid for every x; therefore,

$$M \leq k_m. \tag{3.24}$$

The analysis of the M equation is quite involved, therefore we go through the other equations.

3.2.2 N equation

Then, let's consider the last equation in (3.16) in the region of Supp(P). Supposing that N has a maximum point in z^* such that $N(z^*) > \bar{N} = \frac{\beta}{\zeta}k_m > 0$, we have $N'(z^*) = 0, N''(z^*) < 0$; moreover, if we fix x, then we define

$$t^* = \frac{x - z^*}{a}, \quad M^* = M(t^*;x), \quad N^* = N(z^*),$$
$$P^* = P(z^*) > 0.$$

We have $M^* \leq k_m$ from (3.24), due to the argument done in the previous paragraph for the M equation, and $K_B(N^*)P^* > 0$ since $P^* > 0$ and the K_B function is non-negative. As a result, we deduce that

$$\begin{aligned} D_N N''(z^*) &= -\beta M^* + \gamma K_B(N^*)P^* + \zeta N^* \\ &> -\beta k_m + \gamma K_B(N^*)P^* + \beta k_m = \gamma K_B(N^*)P^* > 0. \end{aligned} \tag{3.25}$$

Thus, there is an absurd, since

$$0 > D_N N''(z^*) > \gamma K_B(N^*)P^* > 0$$

This argument is valid for every x. The solutions of (3.15), coupled with boundary conditions for N (3.21), is monotonically increasing from 0 to $\frac{\beta}{\zeta}k_m$

3.2.3 Regions of analysis: case I

We analyse the travelling wave in two cases: Case I and Case II. Denoting by z_0 where $N = n_k$, in Case I we assume $z_0 < 0$, while in Case II $z_0 > 0$. In this subsection we consider Case I. Thus, we can split the analysis in three regions, as depicted in Fig. 3.2, Region I, II and III. Denoting by z_0 where $N = n_k$, these regions are characterized in the following way:

- Region I: $z \in (-\infty, 0]$, with $N < n_k$;
- Region II: $z \in [z_0, 0]$, with $N > n_k$ for $z > z_0$;
- Region III: $z \in [0, +\infty)$, with $N > n_k$.

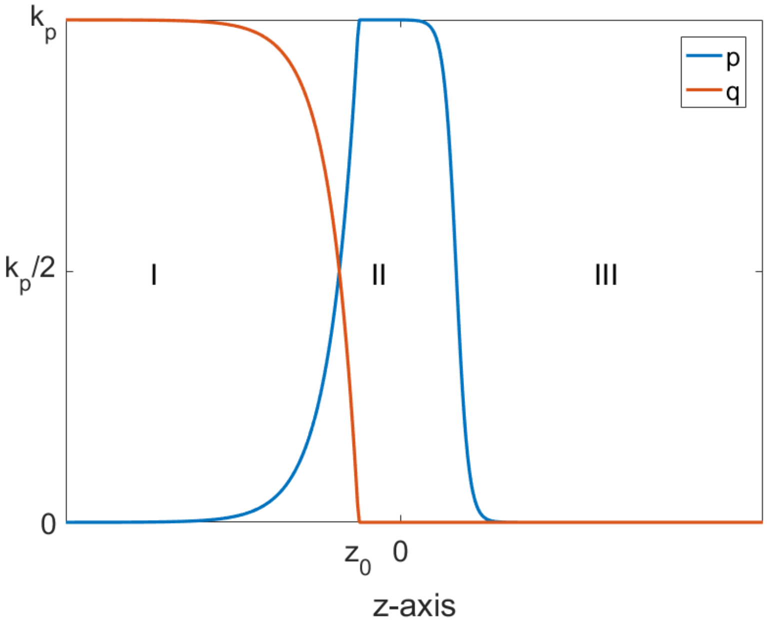

Figure 3.2: Travelling wave regions: p in blue, q in red

From the sum of the first two equations of (3.15) we have

$$-a\,(P+Q)' - (\nu_P\,P\,\Pi')' - (\nu_Q\,Q\,\Pi')' = K_B\,(N)\,P\left(1 - \frac{P+Q}{k_p}\right). \tag{3.26}$$

Multiplying this equation for $\mu\,\Pi$, after some calculations, we obtain:

$$\begin{aligned}-a\Pi'\,(P+Q) = \mu\Pi\,[(\nu_P\,P+\nu_Q\,Q)\,\Pi'' + (\nu_P\,P'+\nu_Q\,Q')\,\Pi' \\ +K_B\,(N)\,P\left(1-\frac{P+Q}{k_p}\right)\right]\end{aligned} \tag{3.27}$$

We can use the maximum principle on the interval $(-\infty, 0)$ applied to (3.26) to recover that, since we have $\Pi\,(-\infty) = \Pi\,(0) = K_\mu\,k_p^\mu$, $\Pi \equiv k_p$ on $(-\infty, 0)$. In fact, if we suppose that $z^* = \operatorname{argmax}_{z\in(-\infty,0)}\Pi$, $\Pi(z^*) > K_\mu\,k_p^\mu$, then we have that

$$\begin{gathered}\Pi\,(z^*) > k_p^\mu, \quad (P+Q)\,(z^*) > k_p, \quad \Pi' = 0, \\ (P+Q)' = 0, \quad \Pi'' < 0, \quad (P+Q)'' < 0.\end{gathered}$$

It follows that we have an absurd, because the right hand side in (3.27) will be negative

$$\begin{aligned}\mu\Pi\,[(\nu_P\,P+\nu_Q\,Q)\,\Pi'' + (\nu_P\,P'+\nu_Q\,Q')\,\Pi' + \\ K_B\,(N)\,P\left(1-\frac{P+Q}{k_p}\right)\right] < \mu\Pi\,[(\nu_P\,P+\nu_Q\,Q)\,\Pi''] < 0,\end{aligned}$$

and the left hand side of the same equation will be zero. Therefore, $\Pi \le K_\mu\,k_p^\mu$ so $P+Q \le k_p$. This implies $P \le k_p, Q \le k_p$. Moreover, if we suppose there is a local minimum for $P+Q$ in $(-\infty, 0)$ greater than k_p, then

$$\Pi' = 0, \quad (P+Q)' = 0, \quad \Pi'' > 0, \quad (P+Q)'' > 0,$$

but this is impossible since the right hand side in (3.27) will be positive

$$\begin{aligned}\mu\Pi\,[(\nu_P\,P+\nu_Q\,Q)\,\Pi'' + (\nu_P\,P'+\nu_Q\,Q')\,\Pi' + \\ K_B\,(N)\,P\left(1-\frac{P+Q}{k_p}\right)\right] > \mu\Pi\,[(\nu_P\,P+\nu_Q\,Q)\,\Pi''] > 0,\end{aligned}$$

and the left hand side of the same equation will be zero. As a consequence, we deduce that on $(-\infty, 0]$

$$P' + Q' = 0, \tag{3.28}$$

and from the boundary conditions we have that on $(-\infty, 0]$

$$P + Q = k_p. \tag{3.29}$$

We start from the Region II to obtain a result useful for the computations in Region I, and then we will proceed in Region III.

Region II Recalling that $P+Q=k_p$, $\Pi'=0, P'+Q'=0$, the system (3.16) can be written as follows:

$$\begin{cases} aP' = -\varepsilon\, Q \\ aQ' = \varepsilon\, Q \\ -aM' = -\alpha P\, M + \eta M\left(1-\dfrac{M}{k_m}\right) \\ -aN' - D_N N'' = \beta\, M - \gamma\, K_B\,(N)\; P - \zeta\, N \end{cases} \tag{3.30}$$

Integrating the first equation in (3.30), this system has the following solutions:

$$P\,(z) = k_p - k\, e^{\frac{\varepsilon}{a}z} Q\,(z) = k\, e^{\frac{\varepsilon}{a}z}, \tag{3.31}$$

with k a constant to be defined with a proper boundary condition. Recalling that $P\,(0)=k_p$, $P+Q=k_p$, we deduce that $Q\,(0)=0$. Then, the differential equation for Q has only the null solution $Q\equiv 0$, so $k=0$. As a result, we have

$$P\equiv k_p, \quad Q\equiv 0. \tag{3.32}$$

Region I Recalling that $P+Q=k_p$, $\Pi'=0, P'+Q'=0$, the system (3.15) can be written as follows:

$$\begin{cases} aP' = \varepsilon P \\ aQ' = -\varepsilon\, P \\ -aM' = -\alpha P\, M + \eta M\left(1-\dfrac{M}{k_m}\right) \\ -aN' - D_N N'' = \beta\, M - \gamma\, K_B\,(N)\; P - \zeta\, N \end{cases} \tag{3.33}$$

with boundary conditions (3.20), (3.18). Integrating the first equation in (3.33), this system has the following solutions:

$$P\,(z) = k\, e^{\frac{\varepsilon}{a}z}, \quad Q\,(z) = k_p - k\, e^{\frac{\varepsilon}{a}z} \tag{3.34}$$

with k a constant to be defined with a proper boundary condition. To this purpose, we can obtain the analytical expression for P and Q in Region I starting from (3.34) and using the boundary conditions of P and Q in z_0 deduced from the analysis in Region II $P\,(z_0)=k_p, Q\,(z_0)=0$:

$$P\,(z) = k_p\, e^{\frac{\varepsilon}{a}(z-z_0)}, \quad Q\,(z) = k_p\left(1-e^{\frac{\varepsilon}{a}(z-z_0)}\right) \tag{3.35}$$

Region III Recalling that $\mathrm{Supp}(Q) \subseteq (-\infty, 0]$, in this region $Q = 0$, and $\Pi = P^{\mu}$. Therefore, the system (3.15) can be written as follows:

$$\begin{cases} -aP' - [P\,\nu_P(P^{\mu})']' = \left[K_B\,(N)\left(1-\dfrac{P}{k_p}\right)\right]P \\ Q = 0 \\ -aM' = -\alpha P\,M + \eta M\left(1-\dfrac{M}{k_m}\right) \\ -aN' - D_N N'' = \beta\,M - \gamma\,K_B\,(N)\;P - \zeta\,N \end{cases} \tag{3.36}$$

We consider now the first equation of the system on $[0, +\infty)$ (3.36):

$$-aP' - [P\,\nu_P\Pi']' = \left[K_B\,(N)\left(1-\frac{P}{k_p}\right)\right]P \tag{3.37}$$

$$P(0) = k_p, \quad P(+\infty) = 0, \quad P'(0) = 0, \quad P'(+\infty) = 0. \tag{3.38}$$

Using the maximum principle on (3.37), Π is monotonically decreasing. Multiplying both sides of (3.37) by Π and using the fact that

$$\Pi\,[\nu_P P\Pi']' = [\Pi\,P\,\nu_P\Pi']' - \nu_P\,P(\Pi')^2$$

we obtain:

$$-a\,P'\,\Pi - [\Pi\,P\,\nu_P\Pi']' + \nu_P\,P(\Pi')^2 = K_B\,(N)\left(1-\frac{P}{k_p}\right)P\,\Pi \tag{3.39}$$

$$P(0) = k_p, \quad P(+\infty) = 0. \tag{3.40}$$

For every $r_1 \geq 0, r_2 > r_1$, integrating over $[r_1, r_2]$ and estimating from above using the fact that

$$\begin{gathered} \Pi, P \text{ are positive and bounded on } (0,+\infty)\,; \\ P\,(+\infty) = 0, \quad \Pi\,(+\infty) = 0; \\ \Pi' < 0, \quad P' < 0 \text{ and bounded on } (0,+\infty)\,; \\ P'(0) = 0, \quad \Pi'\,(0) = 0, \quad c > 0, \end{gathered}$$

and defining

$$f\,(P,N) := K_B\,(N)\left(1-\frac{P}{k_p}\right),$$

we find

$$\int_{r_1}^{r_2} (\nu_P\,P)\,\Pi'^2\,dx \leq \int_{r_1}^{r_2} f\,(P,N)\,P\,\Pi\,dx + [\Pi\,\nu_P P\Pi']_{r_1}^{r_2} < \infty \tag{3.41}$$

Hence, $\Pi' \in L^2\,[(r_1, r_2)]$, so $\Pi' \in L^2_{loc}\,((0,+\infty))$ and, therefore, Π is continuous on $[0, +\infty]$; as a consequence, $P + Q$ is continuous as well. This implies also P is continuous as well.
Furthermore, on $[0, +\infty)$, $Q \equiv 0$.

3.2.4 Regions of analysis: Case II

In this subsection we consider Case II. Thus, we can split the analysis in two regions, as depicted in Fig. 3.3, Region I and II. Denoting by z_0 where $N = n_k$, these regions are characterized in the following way:

- Region I: $z \in (-\infty, 0]$;
- Region II: $z \in [0, +\infty)$.

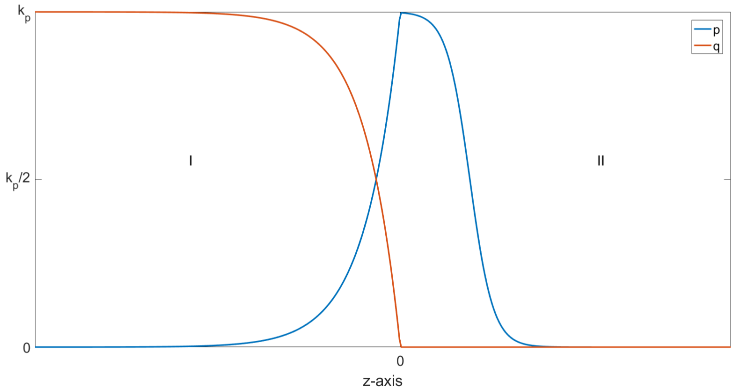

Figure 3.3: Travelling wave regions: p in blue, q in red

We will follow the initial steps illustrated before in the Case I.

Region I From the sum of the first two equations of (3.15) we have

$$-a\,(P+Q)' - (\nu_P\,P\,\Pi')' - (\nu_Q\,Q\,\Pi')' = K_B\,(N)\,P\left(1-\frac{P+Q}{k_p}\right). \tag{3.42}$$

Multiplying this equation for $\mu\,\Pi$, after some calculations, we obtain:

$$-a\Pi'\,(P+Q) = \mu\Pi\left[(\nu_P\,P+\nu_Q\,Q)\,\Pi'' + (\nu_P\,P'+\nu_Q\,Q')\,\Pi' + K_B\,(N)\,P\left(1-\frac{P+Q}{k_p}\right)\right] \tag{3.43}$$

We can use the maximum principle on the interval $(-\infty, 0)$ applied to (3.42) to recover that, since we have $\Pi\,(-\infty) = \Pi\,(0) = K_\mu\,k_p^\mu$, $\Pi \equiv k_p$ on $(-\infty, 0)$. In fact, if we suppose that $z^* = \operatorname{argmax}_{z\in(-\infty,0)}\Pi$, $\Pi(z^*) > K_\mu\,k_p^\mu$, then we have that

$$\Pi\left(z^*\right) > k_p^\mu, \quad (P+Q)\left(z^*\right) > k_p, \quad \Pi' = 0,$$
$$(P+Q)' = 0, \quad \Pi'' < 0, \quad (P+Q)'' < 0.$$

It follows that we have an absurd, because the right hand side in (3.43) will be negative

$$\mu\Pi\left[\left(\nu_P\, P + \nu_Q\, Q\right)\Pi'' + \left(\nu_P\, P' + \nu_Q\, Q'\right)\Pi' + K_B\left(N\right)P\left(1 - \frac{P+Q}{k_p}\right)\right] < \mu\Pi\left[\left(\nu_P\, P + \nu_Q\, Q\right)\Pi''\right] < 0,$$

and the left hand side of the same equation will be zero. Therefore, $\Pi \leq K_\mu\, k_p^\mu$ so $P+Q \leq k_p$. This implies $P \leq k_p, Q \leq k_p$. Moreover, if we suppose there is a local minimum in $(-\infty, 0)$ for $P+Q$ greater than k_p, then

$$\Pi' = 0, \quad (P+Q)' = 0, \quad \Pi'' > 0, \quad (P+Q)'' > 0,$$

but this is impossible since the right hand side in (3.43) will be positive

$$\mu\Pi\left[\left(\nu_P\, P + \nu_Q\, Q\right)\Pi'' + \left(\nu_P\, P' + \nu_Q\, Q'\right)\Pi' + K_B\left(N\right)P\left(1 - \frac{P+Q}{k_p}\right)\right] > \mu\Pi\left[\left(\nu_P\, P + \nu_Q\, Q\right)\Pi''\right] > 0,$$

and the left hand side of the same equation will be zero. As a consequence, we deduce that on $(-\infty, 0]$

$$P' + Q' = 0, \tag{3.44}$$

and from the boundary conditions we have that on $(-\infty, 0]$

$$P + Q = k_p. \tag{3.45}$$

We can recover the analytical expression of P and Q in Region I, since their equations reduce to:

$$\begin{cases} -a\, P' = -\varepsilon P \\ -a\, Q' = \varepsilon P. \end{cases} \tag{3.46}$$

This system has the following solutions:

$$P\left(z\right) = k\, e^{\frac{\varepsilon}{a}z}, \quad Q\left(z\right) = k_p - k\, e^{\frac{\varepsilon}{a}z} \tag{3.47}$$

with k a positive constant to be defined with a proper boundary condition. To this purpose, we can obtain the analytical expression for P and Q in Region I starting from (3.47) and using the boundary conditions of P and Q in 0:

$$P\left(z\right) = k_p\, e^{\frac{\varepsilon}{a}z}, \quad Q\left(z\right) = k_p\left(1 - e^{\frac{\varepsilon}{a}z}\right) \tag{3.48}$$

Region II Recalling that $\mathrm{Supp}(Q) \subseteq (-\infty, 0]$, in this region $Q = 0$, and $\Pi = P^{\mu}$. Therefore, the system (3.15) can be written as follows:

$$\begin{cases} -aP' - [P\,\nu_P(P^{\mu})']' = \left[K_B\,(N)\left(1 - \dfrac{P}{k_p}\right)\right] P \\ Q = 0 \\ -aM' = -\alpha P\,M + \eta M\left(1 - \dfrac{M}{k_m}\right) \\ -aN' - D_N N'' = \beta\,M - \gamma\,K_B\,(N)\;P - \zeta\,N \end{cases} \tag{3.49}$$

We consider now the first equation of the system on $[0, +\infty)$ (3.49):

$$-aP' - [P\,\nu_P \Pi']' = \left[K_B\,(N)\left(1 - \frac{P}{k_p}\right)\right] P \tag{3.50}$$

$$P(0) = k_p, \quad P(+\infty) = 0, \quad P'(0) = 0, \quad P'(+\infty) = 0. \tag{3.51}$$

Using the maximum principle on (3.50), Π is monotonically decreasing. Multiplying both sides of (3.50) by Π and using the fact that

$$\Pi\,[\nu_P P \Pi']' = [\Pi\,P\,\nu_P \Pi']' - \nu_P\,P(\Pi')^2$$

we obtain:

$$-a\,P'\,\Pi - [\Pi\,P\,\nu_P \Pi']' + \nu_P\,P(\Pi')^2 = K_B\,(N)\left(1 - \frac{P}{k_p}\right) P\,\Pi \tag{3.52}$$

$$P(0) = k_p, \quad P(+\infty) = 0. \tag{3.53}$$

For every $r_1 \geq 0, r_2 > r_1$, integrating over $[r_1, r_2]$ and estimating from above using the fact that

$$\begin{gathered} \Pi, P \text{ are positive and bounded on } (0, +\infty)\,; \\ P\,(+\infty) = 0, \quad \Pi\,(+\infty) = 0; \\ \Pi' < 0, \quad P' < 0 \text{ and bounded on } (0, +\infty)\,; \\ P'(0) = 0, \quad \Pi'\,(0) = 0, \quad c > 0, \end{gathered}$$

and defining

$$f\,(P, N) := K_B\,(N)\left(1 - \frac{P}{k_p}\right),$$

we find

$$\int_{r_1}^{r_2} (\nu_P\,P)\,\Pi'^2\,dx \leq \int_{r_1}^{r_2} f\,(P, N)\,P\,\Pi\,dx + [\Pi\,\nu_P P \Pi']_{r_1}^{r_2} < \infty \tag{3.54}$$

Hence, $\Pi' \in L^2\,[(r_1, r_2)]$, so $\Pi' \in L^2_{loc}\,((0, +\infty))$ and, therefore, Π is continuous on $[0, +\infty]$; as a consequence, $P + Q$ is continuous as well. This implies also P is continuous as well.
Furthermore, on $[0, +\infty)$, $Q \equiv 0$.

Chapter 4

Numerical simulations

The code employed to approximate numerically the travelling wave solutions is written in
MATLAB®. We use the function `pdepe` [30] to compute the numerical solution of the complete system (2.5). The code solves initial-boundary value problems for systems of parabolic and elliptic PDEs in the one space variable x and time t. The standard call of the function is:

```
sol = pdepe(m,pdefun,icfun,bcfun,xmesh,tspan)
```

where `pdefun`, `icfun`, `bcfun` are function handles. The ordinary differential equations (ODEs) resulting from discretization in space are integrated to obtain approximate solutions at time intervals specified in `tspan`. The `pdepe` function returns values of the solution on a mesh provided in `xmesh`. `pdepe` solves PDEs of the form:

$$\begin{aligned} c\left(x,t,u,\frac{\partial u}{\partial x}\right)\frac{\partial u}{\partial t} = x^{-m}\frac{\partial}{\partial x}\left(x^m f\left(x,t,u,\frac{\partial u}{\partial x}\right)\right) \\ +s\left(x,t,u,\frac{\partial u}{\partial x}\right). \end{aligned} \tag{4.1}$$

The PDEs hold for $t_0 \leq t \leq t_f$ and $a \leq x \leq b$. The interval $[a,b]$ must be finite. The integer m can be 0, 1, or 2, corresponding to slab, cylindrical, or spherical symmetry, respectively. If $m > 0$, then a must be nonnegative. We choose to set $m = 0$ at the beginning of our code. For $t = t_0$, the solution components takes the initial conditions of the form

$$u\left(x,t_0\right) = u_0\left(x\right)$$

The boundary conditions, for all t and at $x = a$ or $x = b$ are of the following form

$$p\left(x,t,u\right) + q\left(x,t\right) f\left(x,t,u,\frac{\partial u}{\partial x}\right) = 0 \tag{4.2}$$

Note that the boundary conditions are expressed in terms of the flux f rather than $\partial u/\partial x$. Moreover, only p can depend on u.

4.1 Structure of the code

In the file `Tumor1D.m` there are the lines that will call two files. The former call sets the value of the parameters, the latter calls the function `pdex` which computes the solution of the full problem in 1D. The equations to be passed to the solver will be in the non-dimensional form, so the solutions that will be calculated and plotted in the following figures will be non-dimensional.

```
clear all
parameters;
pdex17();
```

In the file `parameters.m` we define all the parameters and their own values. We prefer to define the variables as global in order to share them between the calls to the functions which will be used afterwards.

Listing 4.1: File parameters.m

```
global Dn1 Dn n0 t0 x0 psi Dp0 Dq0 gamma0 q0 p0
   eta beta gamma eps alpha kp khatp chi Dp Dq per
   ro m0 km khatm  cm vmax
t0 = 57600;
x0 = 0.2;

p0 = 10^9 * x0^3; %[cells]
q0 = p0;
n0 = 5* 10^-2*10^-3; %[M]

Dp0 = 10^-9;
Dq0 = Dp0*2;
Dn0 = 2 * 10^-5;

Dp = Dp0*t0/x0^2;
Dq = Dq0*t0/x0^2;
Dn = Dn0*t0/x0^2;

kp = 1.*p0;
khatp = kp/p0;
```

```
chi =0.34*0;
ro = 0.38*0;

m0 = 1;
km = m0;
khatm= km/m0;
alpha = 10;
eta = 0.15;

beta  = 0.3*t0;
gamma   = gamma0*p0/n0;
psi = 0.15*t0;
gamma0 = 2 * 10^-12/32; %[M/cell]
gamma = gamma0*p0/n0;

gammas = 1e-5;

vmax = gammas*t0;

cm = 1.5e-7/32*1000/n0;


% The value of eps tunes the reference value for the quiescent cells;
% per tunes the difference between the proliferating and quiescent cells;

eps = 70;
per = 0.05;
```

The function `pdex` defines the 1D mesh and the time interval, with its discretization to be employed, with the following commands:

```
%% Matlab code
% This file compute the solution for the whole system
% with every component; it uses a linear function for K_B, tanh function for K_{PQ}
%close all
m = 0;
x =linspace(0,1,150);
t = linspace(0,1,200);
```

```
options = odeset('RelTol',1e-6,'AbsTol',1e-7,'BDF'
   ,'on','MaxOrder',5);
sol = pdepe(m,@pdex4pde,@pdex4ic,@pdex4bc,x,t,
   options);
```

In `x` and in `t` we store the discretization of the space and time interval, respectively. In the variable `options`, which can be passed as input to `pdepe`, one can set the values for the relative and absolute tolerance of the solver, to use the Backward Difference Formula (BDF), and eventually its maximum order. The spatial dependence is approximated with Finite Difference Method, while time stepping is adaptive. For time integration, the `pdepe` command uses a variable order multistep solver, based on Gear's method [26]. In the following lines we store the results in 4 different variables, respectively, for $p(x,t), q(x,t), m(x,t), n(x,t)$. Then, we plot a 3-D coloured surface with the command `surf` for every variable.

```
  u1 = sol(:,:,1);
  u2 = sol(:,:,2);
  u3 = sol(:,:,3);
  u4 = sol(:,:,4);
  figure
  s1=surf(x,t,u1)
  title('p(x,t)')
  xlabel('Distance x')
  ylabel('Time t')
  s1.EdgeColor = 'none';
```

At the end, we compare the profiles of the fields p, q, m, n and of $p+q$ at time $t=1$, in order to point out the possible profiles of travelling waves with 1D plots.

```
   figure
  hold on
  plot(x,u1(end,:,1))
  plot(x,u2(end,:,1))
  plot(x,u1(end,:,1)+u2(end,:,1))
  plot(x,u3(end,:,1))
  plot(x,u4(end,:,1))
```

The function `pdepe` uses the function `pdex4bc`, `pdexic`, and `pdex4pde`. First, let's look at the first one:

Listing 4.2: Function `pdex4bc`

```
function [pl,ql,pr,qr] = pdex4bc(xl,ul,xr,ur,t)
pl = [0;0;0;0];
ql = [1; 1; 1; 1];
pr = [0; 0; 0; 0 ];
qr = [1; 1; 1; 1];
```

In our simulations, we will adopt the choice of zero flux on the boundary for all the four equations, respectively of $\hat{p}, \hat{q}, \hat{m}, \hat{n}$. Therefore, we have to define four vectors of length four for the values of the function $p\left(x,t,u\right)$ and $q\left(x,t\right)$ of 4.2.

$$\texttt{pl} = p\left(x_l,t,u\right), \quad \texttt{pr} = p\left(x_r,t,u\right), \quad \texttt{ql} = q\left(x_l,t\right), \quad \texttt{qr} = q\left(x_r,t\right), \\ \texttt{x} = \left(x_l,x_r\right)$$

In our simulations they are, respectively, 0 and 1 on the left and right border of the interval `x`. After that, we define the initial condition in the function `pdexic`:

Listing 4.3: Function `pdex4ic`

```
function u0 = pdex4ic(x);
u0 = [ 0.0015*exp(-0.2*x)*(x<=1); 0; 1; 2];
```

Here, we define the vector `u0` of length four to store the initial values of $p\left(x,0\right), q\left(x,0\right), m\left(x,0\right), n\left(x,0\right)$. Finally, we provide the definition of the functions and equations:

Listing 4.4: Function `pdex4pde`

```
function [c,f,s] = pdex4pde(x,t,u,DuDx)
global Dn1 Dn n0 t0 x0 psi kB Dp0 Dq0 gamma0 q0 p0 eta beta gamma eps alpha kp khatp chi Dp Dq per ro m0 km khatm mu cm vmax

k1 = vmax *(u(4)/(cm+u(4)))*(1-(u(1)+u(2))/khatp);
k2 = vmax *(u(4)/(cm+u(4)));

 kPQ = eps*0.5*(-tanh(50*(u(4)-0.5)) + 1) ;

 kQP = (eps - kPQ);

 mu= 200;
 c = [1; 1;1;1];
```

```
f = [Dp*mu*(mu+1)/mu*(u(1)+u(2))^(mu-1)*u(1),Dp*
   mu*(mu+1)/mu*(u(1)+u(2))^(mu-1)*u(1),-ro*u(1)
   ,-chi*u(1) ; Dq*mu*(mu+1)/mu*(u(1)+u(2))^(mu
   -1)*u(2),Dq*mu*(mu+1)/mu*(u(1)+u(2))^(mu-1)*u
   (2),0,0;0,0,0,0;0,0,0,Dn] * DuDx;
s = [(k1  -  kPQ     )*u(1)+  q0/p0*kQP  *u(2) ;
   kPQ*u(1)*p0/q0 - kQP *u(2)  ;-alpha*u(1)*u(3)+
    eta * u(3)*(1-u(3)/khatm) ;beta* u(3)-gamma*u
   (1)*k2-psi*u(4)  ];
```

First, we define the logistic term $\left(1-\frac{\hat{p}+\hat{q}}{\hat{k}_p}\right)$ with the $\hat{K}_B$ function, in `k1`, then $\hat{K}_B$ with `k2`. After that, we define the function K_{PQ} and K_{QP}, the value of `mu` used for the power law of Π, the vector `c` which stores the coefficient of the values of $c\left(x,t,u,\frac{\partial u}{\partial x}\right)$ of 4.1. Lastly, we define two vector `f` and `s` which are the fluxes and source term in 4.1. Therefore, we have to write in term of the fluxes and sources the terms present in the equations that we want to solve, in this case 2.5.

4.2 Test cases

In this section, we illustrate some numerical examples to investigate how the solution is affected by the parameters and of the functions employed. In particular, in order to see if the profile of the travelling wave is affected, we will see the simulations for:

- no chemotaxis and chemotaxis;
- only chemotaxis;
- only haptotaxis;
- both chemotaxis and haptotaxis.

Then, we will compare the profile of the proliferating and the quiescent cells to see the difference in terms of speed of the travelling waves. In order to do so, we chose a proper time interval to fit all the simulations.
The initial conditions are the following:

$$\hat{p}\,(x,0)=0.0015\,e^{-0.20\,x}\,\mathbb{I}_{x\leq 0.1},\quad \hat{q}\,(x,0)=0,$$
$$\hat{m}\,(x,0)=1,\quad \hat{n}\,(x,0)=2.$$

We impose zero flux boundary condition at the border of the one dimensional space domain $x = (0, L)$. When no further information is provided in the following tests, it is understood that the coefficients introduced in 2.1 and the functions defined in 4.2.1 are used.

4.2.1 No haptotaxis and chemotaxis

We start the analysis considering the following set of function and parameters adopted:

$$\hat{K}_{PQ}(\hat{n}) = \varepsilon \times 0.5\left[1 - \tanh\left(\left(\hat{n} - n_k\right)\right)\right], \tag{4.3}$$

$$\hat{K}_{QP}(\hat{n}) = \varepsilon - \hat{K}_{PQ}(\hat{n}) = \varepsilon \times 0.5\left[1 + \tanh\left(\left(\hat{n} - n_k\right)\right)\right], \tag{4.4}$$

$$\hat{K}_B(\hat{n}) = v_{max}\frac{\hat{n}}{c_m + \hat{n}}, \quad \varepsilon = 70, \quad n_k = 0.1, \quad \mu = 200, \tag{4.5}$$

$$\Pi = K_\mu (p+q)^\mu, \quad K_\mu = \frac{\mu + 1}{\mu}. \tag{4.6}$$

In this subsection we are addressing the problem without chemotaxis and haptotaxis, therefore we put $\hat{\rho} = \hat{\chi} = 0$. The other parameters are taken into account the nondimensionalisation of the problem 2.1. We use the space interval $x = (0, L)$, with $L = 1$, subdivided into $n_x = 150$ subintervals of the same length, while the time interval is $t = (0, T)$, with $T = 1.5$, subdivided into $n_t = 1500$ subintervals. Therefore, we have $\Delta x = \frac{L}{n_x} = 0.0067$, $\Delta t = \frac{T}{n_t} = 0.001$. In Figure 4.1 are reported the numerical solutions of the system. We see that on the left $\hat{p} + \hat{q}$ is equal to 1; moreover, p reaches 1 and it decays to 0 at approximately $x = 0.5$. The numerical solutions are more similar to the travelling wave solution of Case I rather than Case II, because, we observe that the position of $z = 0$ in the framework of the travelling wave, where P starts to decrease, is ahead of z_0, where $N = 0.1$. However, Q does not vanish in z_0 in the numerical solution, as it should be from the analysis. Nevertheless, the other characteristics of the solution match.

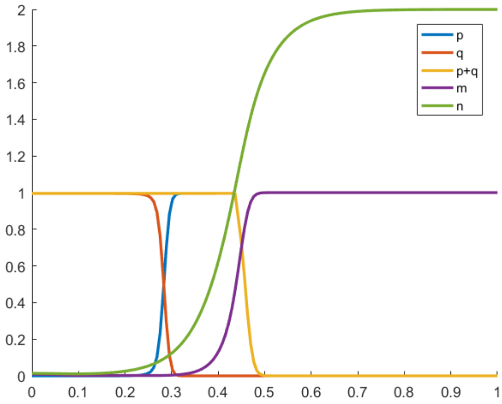

Figure 4.1: Travelling wave without haptotaxis and chemotaxis: $\hat{p}$ in blue, $\hat{q}$ in red, $\hat{p}+\hat{q}$ in yellow, $\hat{m}$ in purple, $\hat{n}$ in green at time $t = 1.5$

In Figure 4.2 there are four pictures showing the travelling wave profiles of the variables overlapped for different time instants.

Remark If $P \equiv 0$ on $[r, +\infty)$, then the equation for M simplifies in

$$M' = -\frac{\eta}{a} M \left(1 - \frac{M}{k_m}\right) \text{ with } M(+\infty) = 0. \tag{4.7}$$

If we suppose that $M(r) < k_m$), then the right hand size of equation (4.7) will be negative, and this implies that $M' < 0$ on $[r, +\infty)$, which leads to an absurd because there is no possibility to match iwth the boundary condition $M(+\infty) = k_m$. As a result, the only solution that can fulfil the boundary condition at $+\infty$ (3.20) is

$$M \equiv k_m \text{ on } [r, +\infty)\,. \tag{4.8}$$

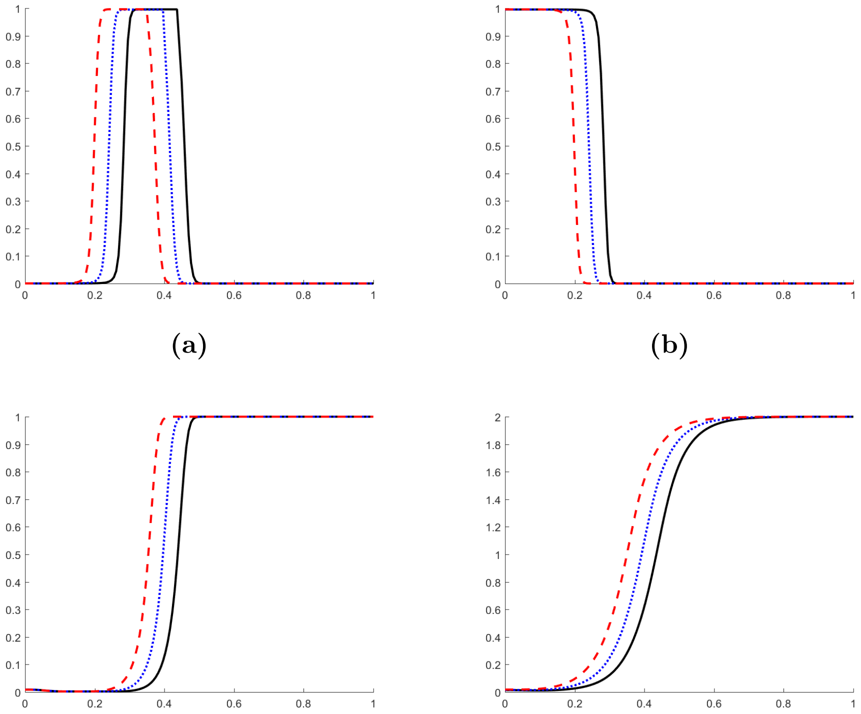

(a) **(b)**

(c) **(d)**

Figure 4.2: Travelling wave profiles of the numerical solutions at $t = 0.7$, $t = 0.85$, $t = 1$ without chemotaxis and haptotaxis: $\hat{p}$ on the top left, $\hat{q}$ on the top right, $\hat{m}$ on the bottom left, $\hat{n}$ on the bottom right. The solutions at $t = 1.2$, $t = 1.35$, $t = 1.5$ are plotted with dashed red line, dotted blue line and solid black line respectively.

4.2.2 Chemotaxis activated

In this case, we keep all the same parameters used in 4.2.1, adding the dimensionless coefficient for the chemotaxis $\hat{\chi} = 0.05$. We choose $x = (0, L)$, with $L = 1$, $n_x = 150$, $t = (0, T)$, with $T = 1$, $n_t = 1000$, so that we have the same Δx, Δt used in 4.2.1.

The system to solve is the following: In Figure 4.3 are reported the numerical solutions. We see that on the left $\hat{p} + \hat{q}$ is approximately to 0.9, sufficiently far from the border $x = 0$; moreover, $\hat{p}$ does not have the same profile of 4.2.1 because, starting from approximately 0 at $x = 0$, it increases, decreases and increases to 1. Finally, it decays to 0 at approximately $x = 0.58$. $\hat{q}$ and $\hat{p}$ have some little oscillations before $x = 0.3$. The profiles of $\hat{m}, \hat{n}$ are smoother than 4.2.1.

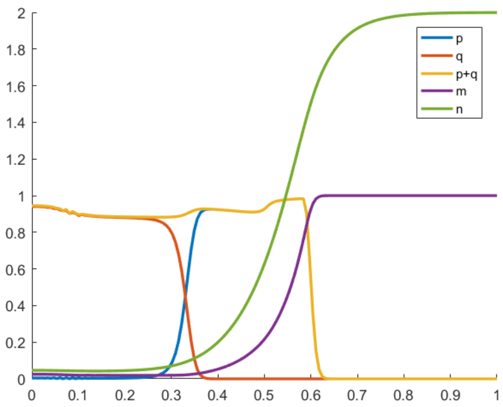

Figure 4.3: Travelling wave with chemotaxis: $\hat{p}$ in blue, $\hat{q}$ in red, $\hat{p}+\hat{q}$ in yellow, $\hat{m}$ in purple, $\hat{n}$ in green at time $t = 1$

In Figure 4.4 there are four pictures showing the travelling wave profiles of the variables overlapped for different time instants.

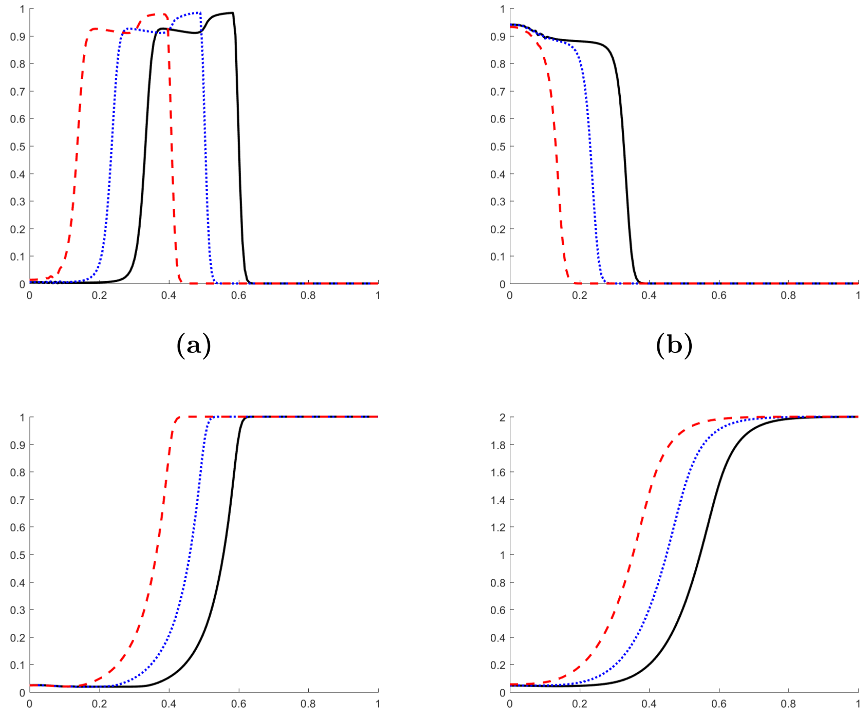

(a) **(b)**

(c) **(d)**

Figure 4.4: Travelling wave profiles of the numerical solutions at $t = 0.7$, $t = 0.85$, $t = 1$ with chemotaxis: $\hat{p}$ on the top left, $\hat{q}$ on the top right, $\hat{m}$ on the bottom left, $\hat{n}$ on the bottom right. The solutions at $t = 0.7$, $t = 0.85$, $t = 1$ are plotted with dashed red line, dotted blue line and solid black line respectively.

4.2.3 Haptotaxis activated

In this case, we keep all the same parameters used in 4.2.1, adding the dimensionless coefficient for the chemotaxis $\hat{\rho} = 0.05$. We use the same $L, \Delta x, T, \Delta t$ of 4.2.2 for the space and time discretization. In Figure 4.5 are reported the numerical solutions. We see that on the left $\hat{p} + \hat{q}$ is approximately to 0.96; moreover, $\hat{p}$ does not have the same profile of 4.2.1 because, starting from approximately 0 at $x = 0$, it increases, decreases and increases to 1. Finally, it decays to 0 at approximately $x = 0.62$. $\hat{q}$ and $\hat{p}$ have some little oscillations before $x = 0.3$. The profiles of $\hat{m}, \hat{n}$ are smoother than 4.2.1.

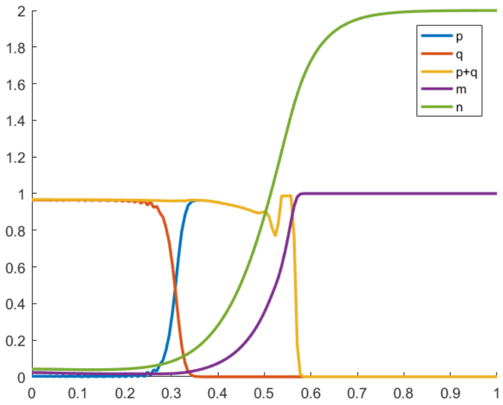

Figure 4.5: Travelling wave with haptotaxis: $\hat{p}$ in blue, $\hat{q}$ in red, $\hat{p}+\hat{q}$ in yellow, $\hat{m}$ in purple, $\hat{n}$ in green at time $t=1$

In Figure 4.6 there are four pictures showing the travelling wave profiles of the variables overlapped for different time instants.

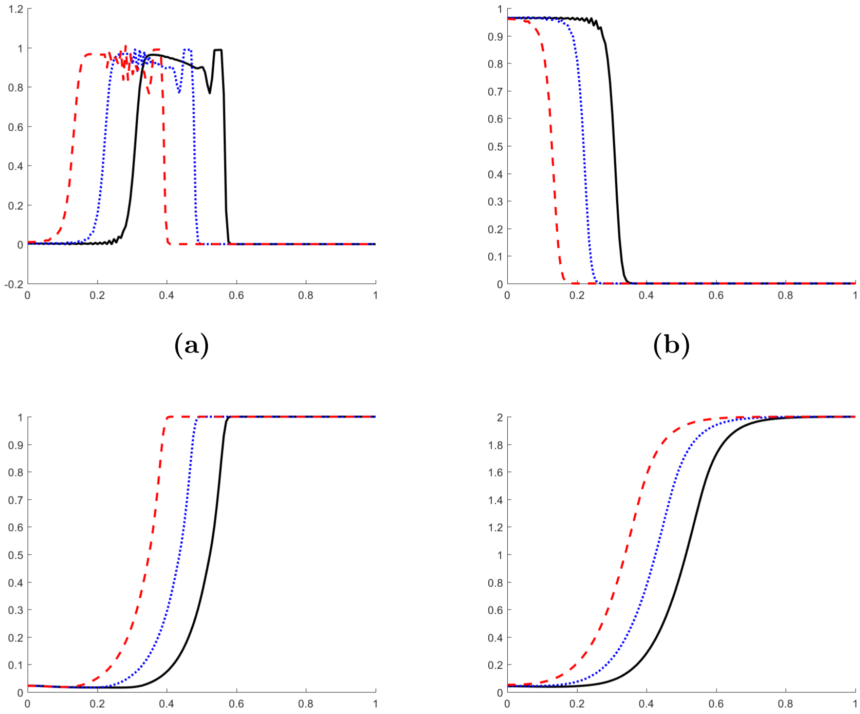

(a) **(b)**

(c) **(d)**

Figure 4.6: Travelling wave profiles of the numerical solutions at $t = 0.7$, $t = 0.85$, $t = 1$ with haptotaxis: $\hat{p}$ on the top left, $\hat{q}$ on the top right, $\hat{m}$ on the bottom left, $\hat{n}$ on the bottom right. The solutions at $t = 0.7$, $t = 0.85$, $t = 1$ are plotted with dashed red line, dotted blue line and solid black line respectively.

4.2.4 Chemotaxis and Haptotaxis activated

In this case, we keep all the same parameters used in 4.2.1, adding the dimensionless coefficient for the chemotaxis $\hat{\rho} = 0.05$, $\hat{\chi} = 0.05$. We use the same $L, \Delta x, T, \Delta t$ of 4.2.2, 4.2.3 for the space and time discretization. In Figure 4.7 are reported the numerical solutions. We see that on the left $\hat{p}+\hat{q}$ is approximately to 0.9; moreover, $\hat{p}$ does not have the same profile of 4.2.1 because, starting from approximately 0 at $x = 0$, it increases, decreases and increases to 1. Finally, it decays to 0 at approximately $x = 0.62$. $\hat{q}$ and $\hat{p}$ have some little oscillations before $x = 0.8$. The profiles of $\hat{m}, \hat{n}$ are smoother than 4.2.1. This solution takes into account all the effects of the haptotaxis and chemotaxis, as a result the front of the travelling wave is more ahead than in 4.2.2, 4.2.3.

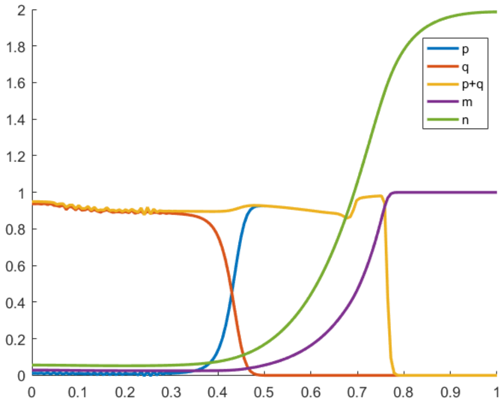

Figure 4.7: Travelling wave with haptotaxis and chemotaxis: $\hat{p}$ in blue, $\hat{q}$ in red, $\hat{p}+\hat{q}$ in yellow, $\hat{m}$ in purple, $\hat{n}$ in green at time $t = 1$

In Figure 4.8 there are four pictures showing the travelling wave profiles of the variables overlapped for different time instants.

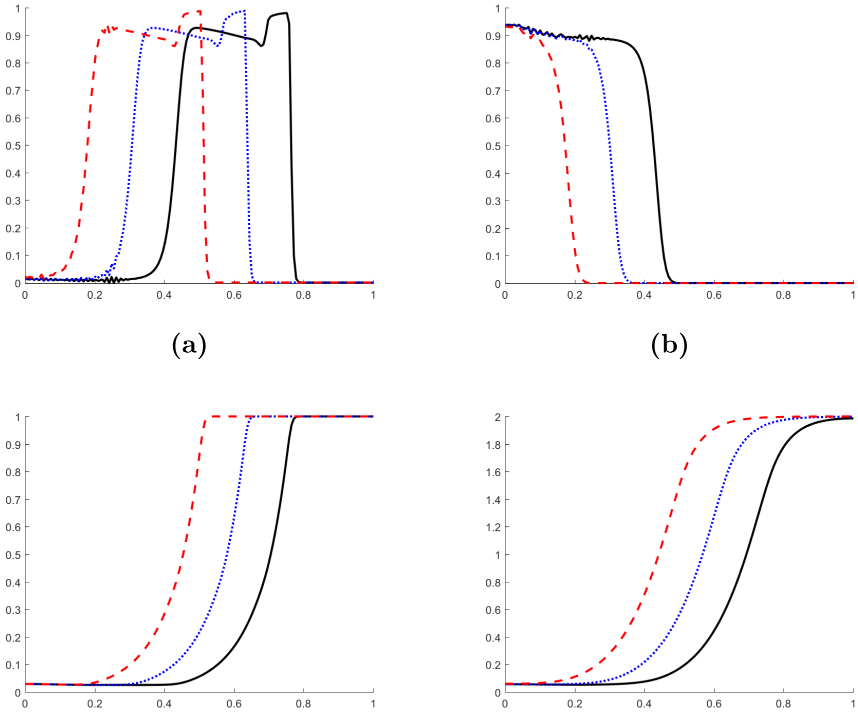

(a) **(b)**

(c) **(d)**

Figure 4.8: Travelling wave profiles of the numerical solutions at $t = 0.7$, $t = 0.85$, $t = 1$ with chemotaxis and haptotaxis: $\hat{p}$ on the top left, $\hat{q}$ on the top right, $\hat{m}$ on the bottom left, $\hat{n}$ on the bottom right. The solutions at $t = 0.7$, $t = 0.85$, $t = 1$ are plotted with dashed red line, dotted blue line and solid black line respectively.

4.2.5 Comparison of profiles

We want to see the differences between the profiles of $\hat{p}$ and $\hat{q}$ in the cases examined before. Only the numerical simulation without chemotaxis and haptotaxi preserves the monotonicity of $\hat{p}$, while all the other present numerical oscillations, which are more enhanced in the case of only haptotaxis. If we combine both the effects of chemotaxis and haptotaxis, the numerical solution is more regular, but still not monotone and with some oscillations in the $\hat{q}$ profile.

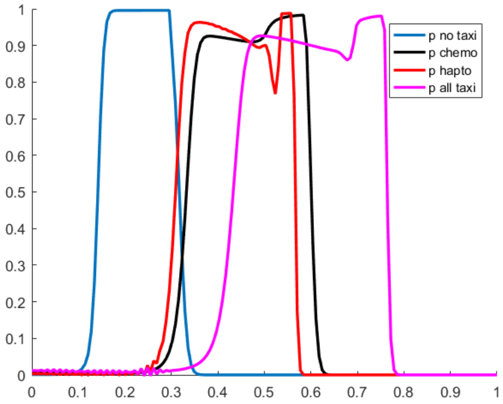

Figure 4.9: $\hat{p}$ at time $t = 1$

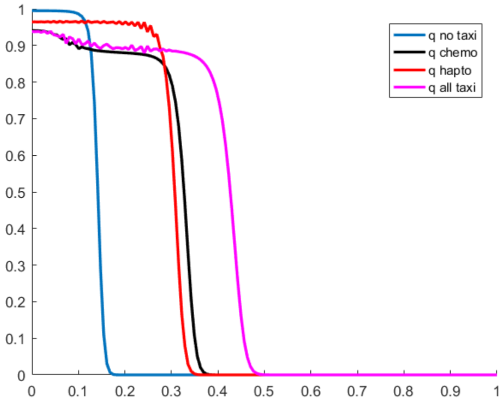

Figure 4.10: $\hat{q}$ at time $t = 1$

4.2.6 Simulations with increased ν_P and ν_Q

In this subsection we repeat the numerical simulation with the same set of parameters used above, except for the random motility coefficients ν_P, ν_Q, which are now 1000 times bigger than in 4.2.1. The following tests investigate if it is possible to recover the monotonicity for p, where $q = 0$.

No haptotaxis and chemotaxis

In the Figure 4.11 we can see that the numerical solution profile without chemotaxis and haptotaxis. In particular, we choose to use $x = (0, L)$, with $L = 1$, $n_x = 150$, $t = (0, T)$, with $T = 1$, $n_t = 1000$, so that we have the same Δx, Δt used in 4.2.1.

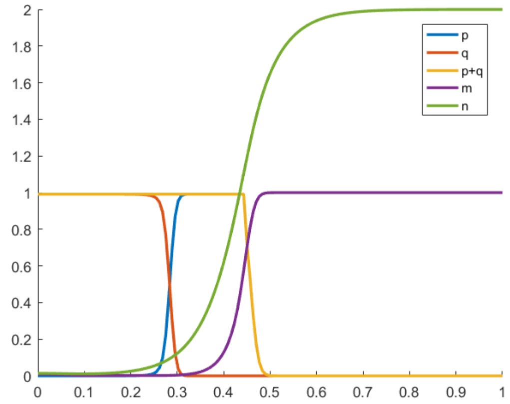

Figure 4.11: Travelling wave without haptotaxis and chemotaxis: $\hat{p}$ in blue, $\hat{q}$ in red, $\hat{p} + \hat{q}$ in yellow, $\hat{m}$ in purple, $\hat{n}$ in green at time $t = 1.5$

The only small noticeable difference between this result and 4.2.1 is a little shift to the right of $\hat{p} + \hat{q}$ front peak.

Haptotaxis activated

In the Figure 4.12 we can see that the numerical solution profile with haptotaxis. In particular, we choose to use $x = (0, L)$, with $L = 1$, $n_x = 150$, $t = (0, T)$, with $T = 1.5$, $n_t = 1500$, so that we have the same Δx, Δt used in 4.2.1.

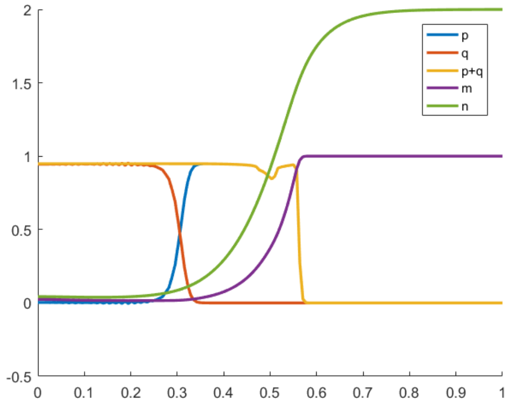

Figure 4.12: Travelling wave with haptotaxis: $\hat{p}$ in blue, $\hat{q}$ in red at time $t = 1.5$

In this case we appreciate a remarkable difference to 4.2.3. In fact, now the sum of proliferating and quiescent cells is constant at the tail of the wave, while in 4.2.3 it was affected by some oscillations. Moreover, the monotonicity of $\hat{p}$ is not recovered, instead there is local minimum and then a local maximum near the wavefront.

Chemotaxis activated

In the Figure 4.13 we can see that the numerical solution profile with chemotaxis. In particular, we choose to use $x = (0, L)$, with $L = 1$, $n_x = 150$, $t = (0, T)$, with $T = 1.5$, $n_t = 1500$, so that we have the same Δx, Δt used in 4.2.1.

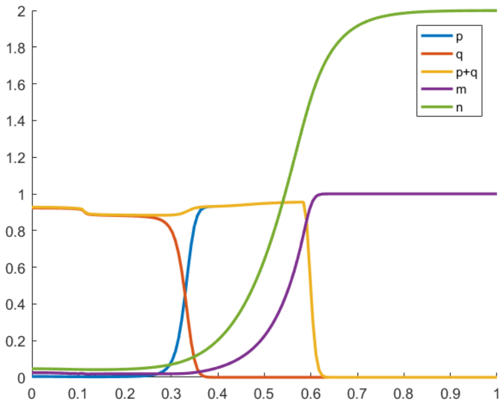

Figure 4.13: Travelling wave with chemotaxis: $\hat{p}$ in blue, $\hat{q}$ in red at time $t = 1.5$

In this case we appreciate a remarkable difference to 4.2.2. In fact, now the sum of proliferating and quiescent cells is no more affected by oscillations at the tail of the wave with respect to 4.2.3. Moreover, the monotonicity of $\hat{p}$ is recovered because there is a smoothing effect near the wavefront due to the increased random motility.

Chemotaxis and Haptotaxis activated

In the Figure 4.14 we can see that the numerical solution profile with haptotaxis and chemotaxis. In particular, we choose to use $x = (0, L)$, with $L = 1$, $n_x = 150$, $t = (0, T)$, with $T = 1.5$, $n_t = 1500$, so that we have the same Δx, Δt used in 4.2.1.

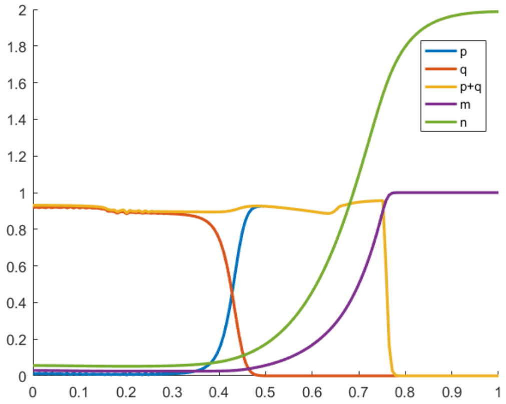

Figure 4.14: Travelling wave with chemotaxis and haptotaxis: $\hat{p}$ in blue, $\hat{q}$ in red at time $t = 1.5$

In this case we can observe both the effects of chemotaxis and haptotaxis. In particular, the numerical oscillations are smoothened, yet the $\hat{p}$ profile is not yet recovered, since there is a local minimum near the wavefront.

4.2.7 Simulations with $\nu_P = \nu_Q$

In this subsection we repeat the numerical simulation with the same set of parameters used above, except for the random motility coefficients ν_P, ν_Q, which are now equal each other to $10^{-}9$ cm^2 s$^{-}1$. In this case, we investigate if the profiles of proliferating and quiescent cells is independent on the relationship between ν_P and ν_Q.

No haptotaxis nor chemotaxis

In the Figure 4.15 we can see that the numerical solution profile without chemotaxis and haptotaxis. In particular, we choose to use $x = (0, L)$, with $L = 1$, $n_x = 150$, $t = (0, T)$, with $T = 1.5$, $n_t = 1500$, so that we have the same Δx, Δt used in 4.2.1.

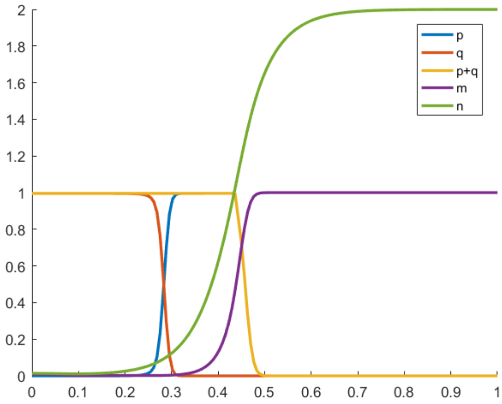

Figure 4.15: Travelling wave without haptotaxis and chemotaxis: $\hat{p}$ in blue, $\hat{q}$ in red, $\hat{p}+\hat{q}$ in yellow, $\hat{m}$ in purple, $\hat{n}$ in green at time $t = 1.5$

In this test we can't appreciate any difference in the profiles with respect to 4.2.1.

Haptotaxis activated

In the Figure 4.16 we can see that the numerical solution profile with haptotaxis. In particular, we choose to use $x = (0, L)$, with $L = 1$, $n_x = 150$, $t = (0, T)$, with $T = 1$, $n_t = 1000$, so that we have the same Δx, Δt used in 4.2.1.

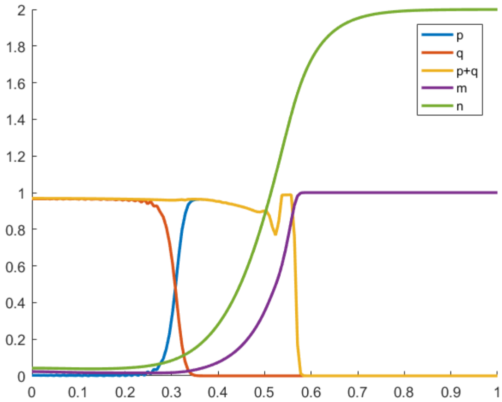

Figure 4.16: Travelling wave with haptotaxis: $\hat{p}$ in blue, $\hat{q}$ in red, $\hat{p}+\hat{q}$ in yellow, $\hat{m}$ in purple, $\hat{n}$ in green at time $t = 1$

Again, we can't appreciate any difference in the profiles with respect to 4.2.3.

Chemotaxis activated

In the Figure 4.17 we can see that the numerical solution profile with haptotaxis. In particular, we choose to use $x = (0, L)$, with $L = 1$, $n_x = 150$, $t = (0, T)$, with $T = 1$, $n_t = 1000$, so that we have the same Δx, Δt used in 4.2.1.

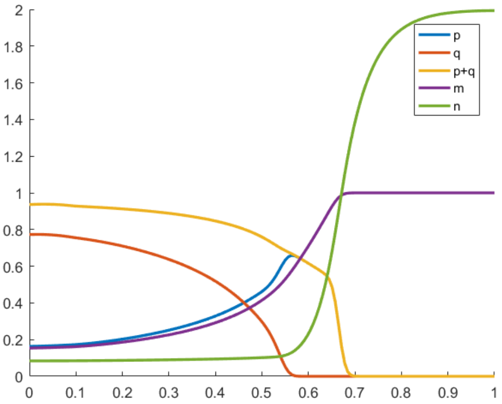

Figure 4.17: Travelling wave with chemotaxis: $\hat{p}$ in blue, $\hat{q}$ in red, $\hat{p} + \hat{q}$ in yellow, $\hat{m}$ in purple, $\hat{n}$ in green at time $t = 0.7$

In this case, the travelling wave profile of the numerical solutions are remarkably different from 4.2.2. In fact, the normalized oxygen concentration reaches a not null steady state at the tail of the wave; the normalized ECM concentration does not reach the steady state since the we are not able to clearly identify the steady state. Moreover, $\hat{p}, \hat{p} + \hat{q}, \hat{q}$ do not reach the unit value.

Chemotaxis and Haptotaxis activated

In the Figure 4.18 we can see that the numerical solution profile with haptotaxis. In particular, we choose to use $x = (0, L)$, with $L = 1$, $n_x = 150$, $t = (0, T)$, with $T = 0.9$, $n_t = 900$, so that we have the same Δx, Δt used in 4.2.1. In Figure 4.18 there is the numerical solutions of this test.

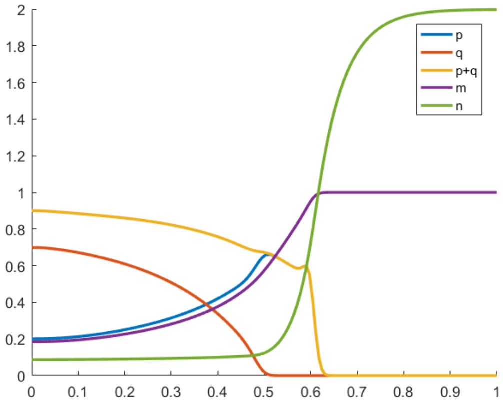

Figure 4.18: Travelling wave with haptotaxis and chemotaxis: $\hat{p}$ in blue, $\hat{q}$ in red, $\hat{p} + \hat{q}$ in yellow, $\hat{m}$ in purple, $\hat{n}$ in green at time $t = 0.6$

We can observe a combination of the effects of chemotaxis and haptotaxis on the travelling wave profiles, which are different with respect to 4.2.4. Moreover, the monotonicity of $\hat{p}$ is not recovered, instead there is local minimum and then a local maximum near the wavefront.

4.2.8 Simulations with different $\hat{\rho}$ and $\hat{\chi}$

In this framework, we investigate the dependence on the chemotactic and haptotactic rates. We'll adopt two values that are different for many orders of magnitude in the case of only haptotaxis and only chemotaxis.

Haptotaxis activated

First, we choose to examine the solutions for $\hat{\rho} = 0.005, 0.1$. In addition, we choose $x = (0, L)$, with $L = 1$, $n_x = 150$, $t = (0, T)$, with $T = 1.5$, $n_t = 1500$, so that we have the same Δx, Δt used in 4.2.1.

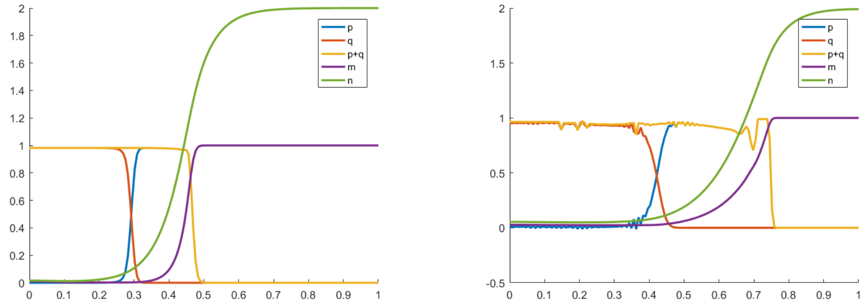

(a) **(b)**

Figure 4.19: Travelling wave profiles of the numerical solutions with haptotaxis: $\hat{p}$ in blue, $\hat{q}$ in red, $\hat{p}+\hat{q}$ in yellow, $\hat{m}$ in purple, $\hat{n}$ in green. On the left, there is the case with $\hat{\rho} = 0.005$ at $t = 1.5$, whereas on the right $\hat{\rho} = 0.1$ at $t = 1$

From Figure 4.19, we can observe that the solution with lower value of $\hat{\rho}$ looks like the case without haptotaxis and chemotaxis. Moreover, the only small difference can be tracked in a little drop of $\hat{p}$ at the wavefront. On the other hand, the solution with higher value of $\hat{\rho}$ have a bigger region where $\hat{p}$ is closer to 1, but there are more numericals oscillations affecting $\hat{p}, \hat{q}$ with respect to 4.2.3.

Chemotaxis activated

The second test we want to carry on is to examine the solutions for $\hat{\chi} = 0.013, 0.1$. In addition, we choose $x = (0, L)$, with $L = 1$, $n_x = 150$, $t = (0, T)$, with $T = 1.5$, $n_t = 1500$, so that we have the same Δx, Δt used in 4.2.1.

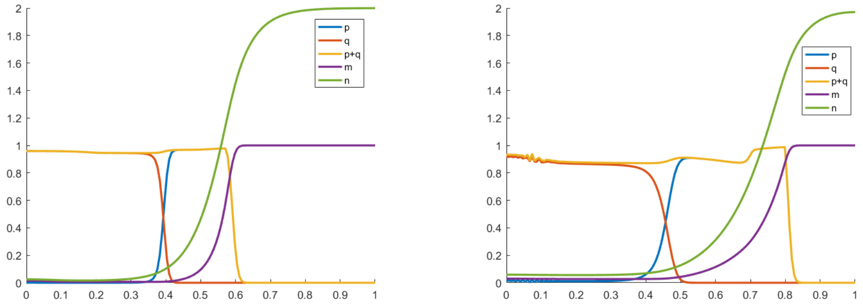

(a) (b)

Figure 4.20: Travelling wave profiles of the numerical solutions with haptotaxis: $\hat{p}$ in blue, $\hat{q}$ in red, $\hat{p}+\hat{q}$ in yellow, $\hat{m}$ in purple, $\hat{n}$ in green. On the left, there is the case with $\hat{\chi} = 0.013$ at $t = 1.5$, whereas on the right $\hat{\chi} = 0.1$ at $t = 1$

From Figure 4.20, we can observe that the solution with a lower value of $\hat{\chi}$ looks like the case without haptotaxis and chemotaxis. Moreover, the only small difference can be tracked in the region of interface of $\hat{p}, \hat{q}$, since the sum of the two increases a bit, remaining smaller than 1.
On the other hand, the solution with higher value of $\hat{\chi}$ have a bigger region where $\hat{p}$ is closer to 1, but the numerical oscillations affecting $\hat{p}, \hat{q}$ are a bit more enhanced with respect to 4.2.2.

4.2.9 Rates of oxygen

In this framework, we are interested in the rates related to the oxygen. In particular, we change the value of the decay and consumption rates $\hat{\zeta}, \hat{\gamma}$ of oxygen, respectively, only for the case without chemotaxis and haptotaxis.

Decay rate

We choose $\hat{\zeta} = \hat{\beta} = 0.3 \times t_0$, $x = (0, L)$, with $L = 1$, $n_x = 150$, $t = (0, T)$, with $T = 1.7$, $n_t = 1700$, so that we have the same Δx, Δt used in 4.2.1.

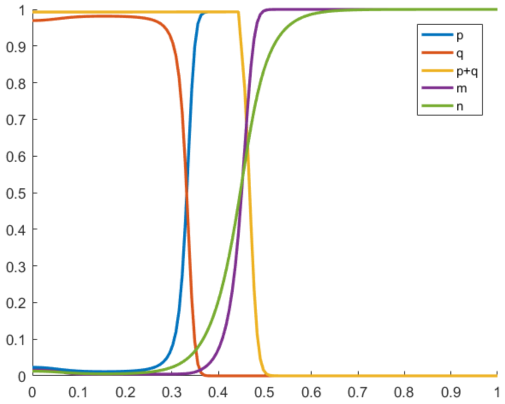

Figure 4.21: Travelling wave without haptotaxis and chemotaxis: $\hat{p}$ in blue, $\hat{q}$ in red, $\hat{p}+\hat{q}$ in yellow, $\hat{m}$ in purple, $\hat{n}$ in green at time $t = 1.7$

In Figure 4.21 there are the numerical solutions. In particular, we can observe that the equilibrium state of the oxygen near the wavefront is different from 4.2.1, because we recall $\bar{N} = \frac{\beta}{\zeta}k_m$, and so now we have $\bar{N} = 1$. Furthermore, the region where $\hat{p}$ is approximately 1 is smaller than in 4.2.1. Finally, the profile of $\hat{q}+\hat{p}$ can't be approximated with $\hat{q}$ at the tail of the wave, because now $\hat{p}$ is no more negligible.

Consumption rate

We choose to increase sensibly the consumption rate, because in 4.2.1 it was smaller for many orders of magnitude with respect to the decay and production rates $\hat{\zeta}, \hat{\beta}$. So, we choose to increase the consumption rate by a factor of $2 \times 10^1 0$, so now $\hat{\gamma} = 7.8124 \times 10^4$, $x = (0, L)$, with $L = 1$, $n_x = 150$, $t = (0, T)$, with $T = 1.5$, $n_t = 1500$, so that we have the same Δx, Δt used in 4.2.1.

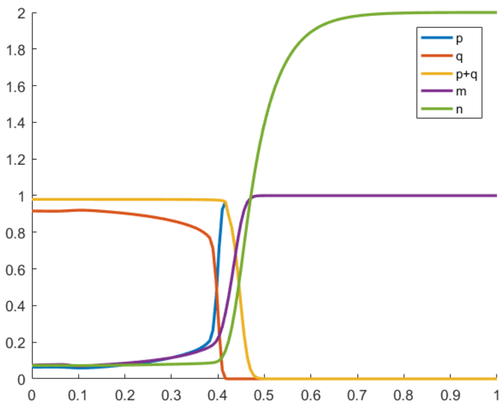

Figure 4.22: Travelling wave without haptotaxis and chemotaxis: $\hat{p}$ in blue, $\hat{q}$ in red, $\hat{p}+\hat{q}$ in yellow, $\hat{m}$ in purple, $\hat{n}$ in green at time $t = 1.5$

In Figure 4.22 there are the numerical solutions. The steady state at the tail of the wave of the wave is not fully developed. Thus, $\hat{M}, \hat{N}, \hat{P}$ are not paltry. Furthermore, the region where $\hat{p}$ is approximately 1 is smaller than in 4.2.1, and $\hat{p}$ profile is more abrupt near the wavefront. Finally, we can't approximate the profile of $\hat{q}+\hat{p}$ with only $\hat{q}$ at the tail of the wave, because now $\hat{p}$ is no more negligible.

Conclusions and Future Work

In this work we have developed and analysed a model for avascular tumour growth. The model reads as system of four nonlinear coupled partial differential equations for four species: the proliferating and quiescent tumour cells, the extracellular matrix and the oxygen concentration. We have found that a travelling wave may exist with appropriate boundary conditions. The numerical simulations are in agreement with the theoretical result about the existence of a travelling wave solution of the system. In particular, the travelling wave solution is characterized by the following properties, depicted in the theoretical analysis (Case I, under the hypothesis $z_0 < 0$):

- Q is a continuous function, exponentially decreasing for $z < z_0$, with $\lim\limits_{z \to -\infty} Q(z) = k_p$, and null for $z > z_0$;
- P is a continuous function, exponentially increasing for $z < z_0$, with maximum value k_p; it takes the constant value k_p for $z_0 < z < 0$ and it is a monotone decreasing function for $z > z_0$;
- $P + Q$ is a continuous function; it takes the constant value k_p for $z < z_0$, and it is equal to P for $z > z_0$;
- N is a continuous monotone increasing function from 0 to $\bar{N} = \frac{\beta}{\zeta} k_m$.

In Case II, under the hypothesis $z_0 > 0$, instead, the system is characterized by the following properties, as pointed out in the theoretical analysis:

- Q is a continuous function, exponentially decreasing for $z < 0$, with $\lim\limits_{z \to -\infty} Q(z) = k_p$, and null for $z > 0$;
- P is a continuous function, exponentially increasing for $z < 0$, it takes the maximum value k_p and it is monotonically decreasing function for $z > 0$;

- $P + Q$ is a continuous function, it takes the constant value k_p for $z < 0$, and it is equal to P for $z > 0$;
- N is a continuous monotone increasing function from 0 to $\bar{N} = \frac{\beta}{\zeta} k_m$.

The numerical simulations are performed in MATLAB using finite difference scheme in space and BDF in time through the `pdepe` solver. The numerical solution in the test case without chemotaxis and haptotaxis approximate to the travelling wave solution of Case I. However, Q does not vanish in z_0 (see Fig 4.1) in the numerical solution, as it is expected from the analysis. Thus, the numerical support of Q is larger than the theoretical one. Nevertheless, the other characteristics of the solution match.

Using the biological parameters available for the parameters relative to the model equations, the tumour growth in the avascular phase asymptotically reaches approximately the diameter of 2 mm in 50 days.

In particular, we can observe that the proliferating cells mainly occupy the outer section of the tumour, while the quiescent cells the inner part. In our case, we don't handle a three population model for tumour cells, i.e. necrotic, quiescent and proliferating cells, but a two population model for tumour cells. In our study the biological and experimentally observable necrotic core and the nearby annular region of quiescent cells are occupied only by quiescent cells. However, the dynamics and the profile of the numerical simulations depend on the presence of haptotaxis and chemotaxis. In fact, the numerical profile of the proliferating and quiescent cells can lose regularity because the problem, with a sufficiently high value of the chemotactic and haptotactic coefficient, is dominated by advection terms. This phenomenon could be avoided employing a more advanced numerical scheme which is able to handle problem dominated by advection.

In addition, we can notice that the travelling wave speed is increased with haptotaxis and chemotaxis since their effect is to model the movement of cells towards higher values of ECM and oxygen concentration.

The increase of the coefficients ν_P, ν_Q leads to a regularising effect on the profile of proliferating and quiescent cells in the numerical simulations. Moreover, the simulations with chemotaxis activated depend on the discrepancy between the two random motility coefficients. In fact, only the numerical solutions, reported in Figures 4.17, 4.18, show evidence of the discrepancy from the profiles where the diffusion coefficients are different each other.

The increase in the values of the chemotactic and haptotactic coefficients yields a bigger rim of proliferating cells in the outer region of the tumour. The variation of the rates related to the oxygen leads to a different profile for the oxygen concentration, because its equilibrium state depends on the production and decay rates β, ζ. Moreover, if we increase the consumption rate, the numerical solution can't be exactly viewed as a travelling wave in the theoretical framework depicted in 3.2, because the ECM, oxygen concentration and proliferating cells are not negligible at the tail of the wave.

The analysis carried out in this work can be further extended in several ways:

- study the existence and characterization of travelling wave solutions in the presence of chemotaxis and haptotaxis;
- improve the accuracy of the numerical scheme adopted to solve the system of equations, to remove the instabilities that appear in the case of strong advection;
- develop numerical simulations in two dimensions, which are much closer to experimental results in terms of pattern formation and evolution.

Bibliography

[1] Gerstman B. *Research on the Physics of Cancer : A Global Perspective.* World Scientific Pub, 2016, pp. 106–107.

[2] Enderling H. and Chaplain M. A. J. “Mathematical Modeling of Tumor Growth and Treatment”. In: *Current Pharmaceutical Design* 20 (2014), pp. 4934–4940.

[3] Meral G. and Surulescu C. “Mathematical modelling, analysis and numerical simulations for the influence of heat shock proteins on tumour invasion”. In: *Journal of Mathematical Analysis and Applications* 408.2 (2013), pp. 597–614.

[4] Papadogiorgaki M., Koliou P., Kotsiakis X., and Zervakis M. E. “Mathematical modelling of spatio-temporal glioma evolution”. In: *Theoretical Biology and Medical Modelling* 10.1 (2013), p. 47.

[5] Tang M., Vauchelet N., Cheddadi I., Vignon-Clementel I., Drasdo D., and Perthame B. “Composite waves for a cell population system modelling tumor growth and invasion”. In: *Chinese Annals of Mathematics - Series B* 34B.2 (2013), pp. 295–318.

[6] Moghaddasi F. L. and Bezak E. and Marcu L. G. “*In Silico* Modelling of Tumour Margin Diffusion and Infiltration: Review of Current Status”. In: *Comp. Math. Methods in Medicine* 2012 (2012), 672895:1–672895:16.

[7] Tindall M. J., Dyson L., Smallbone K., and Maini P. K. “Modelling acidosis and the cell cycle in multicellular tumour spheroids”. In: *J. Theor. Biol.* 298 (2012), pp. 107–115.

[8] Hanahan D. and Weinberg R. A. “Hallmarks of cancer: the next generation”. In: *Cell* 144".5 (2011), pp. 646–674.

[9] Andasari V., Gerisch A., Lolas G., South A. P., and Chaplain M. A. J. “Mathematical modeling of cancer cell invasion of tissue: biological insight from mathematical analysis and computational simulation”. In: *Journal of Mathematical Biology* 63 (2011), pp. 141–171.

[10] Byrne H. M. “Dissecting cancer through mathematics: from the cell to the animal model”. In: *Nat. Rev. Cancer* 10.3 (2010), pp. 221–230.

[11] O’Connor C. M. and Adams J. U. “Cell Division and Cancer”. In: *Nature Education(Scitable)* (2010).

[12] Radszuweit M., Block M., Hengstler J. G., Scholl E., and Drasdo D. “Comparing the growth kinetics of cell populations in two and three dimensions”. In: *Phys. Rev. E* 79 (5 2009), p. 051907.

[13] Gerisch A. and Chaplain M. A. J. “Mathematical modelling of cancer cell invasion of tissue: local and non-local models and the effect of adhesion”. In: *J. Theor. Biol.* 250.4 (2008), pp. 684–704.

[14] Byrne H. M. and Drasdo D. “Individual-based and continuum models of growing cell populations: a comparison”. In: *Journal of Mathematical Biology* 58.4 (2008), 657".

[15] Weinberg R. A. *The Biology of Cancer.* Garland Science, 2007, pp. 643–647.

[16] Chaplain M. A. J. and Lolas G. “Mathematical modelling of cancer invasion of tissue: Dynamic heterogeneity”. In: *Networks and Heterogeneous Media* 1.3 (2006), pp. 399–439.

[17] Chaplain M. A. J. and Lolas G. “Mathematical modelling of cancer invasion of tissue: the role of the urokinase plasminogen activation system”. In: *Mathematical Models and Methods in Applied Sciences* 15.11 (2005), pp. 1685–1734.

[18] Anderson A. R. “A hybrid mathematical model of solid tumour invasion: the importance of cell adhesion”. In: *Math Med Biol* 22.2 (2005), pp. 163–186.

[19] Friedman A. “A hierarchy of cancer models and their mathematical challenges”. In: *Discrete Contin. Dyn. Syst., Ser. B* (2004), pp. 147–159.

[20] Ambrosi D. and Mollica F. “The role of stress in the growth of a multicell spheroid”. In: *Journal of Mathematical Biology* 48.5 (2004), pp. 477–499.

[21] Ambrosi D. and Preziosi L. “On the closure of mass balance models for tumor growth”. In: *Mathematical Models and Methods in Applied Sciences* 12.05 (2002), pp. 737–754.

[22] Dormann S. and Deutsch A. “Modeling of self-organized avascular tumor growth with a hybrid cellular automaton”. In: *In Silico Biol. (Gedrukt)* 2.3 (2002), pp. 393–406.

[23] Hanahan D. and Weinberg R. A. “The hallmarks of cancer”. In: *Cell* 100.1 (2000), pp. 57–70.

[24] Anderson A. R., Chaplain M. A. J., Newman E. L., Steele R. J., and Thompson A. M. “Mathematical Modelling of Tumour Invasion and Metastasis”. In: *Journal of Therotical Medicine* 2.2 (2000), pp. 129–154.

[25] Friedman A. and Reitich F. “Analysis of a mathematical model for the growth of tumors”. In: *J. Math. Biol.* 38.3 (1999), pp. 262–284.

[26] Shampine L. F., Reichelt M. W., and Kierzenka J. A. “Solving Index-1 DAEs in MATLAB and Simulink”. In: *SIAM Review* 41.3 (1999), pp. 538–552.

[27] Ward J. P. and King J. R. “Mathematical modelling of avascular-tumour growth”. In: *IMA J Math Appl Med Biol* 14.1 (1997), pp. 39–69.

[28] Byrne H. M. and Chaplain M. A. J. “Growth of nonnecrotic tumors in the presence and absence of inhibitors”. In: *Math. Biosci.* 130.2 (1995), pp. 151–181.

[29] Casciari J. J., Sotirchos S. V., and Sutherland R. M. “Variations in tumor cell growth rates and metabolism with oxygen concentration, glucose concentration, and extracellular pH”. In: *J. Cell. Physiol.* 151.2 (1992), pp. 386–394.

[30] Skeel R. D. and Berzins M. “A Method for the Spatial Discretization of Parabolic Equations in One Space Variable”. In: *SIAM Journal on Scientific and Statistical Computing* 11.1 (1990), pp. 1–32.

[31] Maini P. K. “Spatial and spatio-temporal patterns in a cell-haptotaxis model”. In: *J. Math. Biol.* 27.5 (1989), pp. 507–522.

[32] Freyer J. P. and Sutherland R. M. “Regulation of Growth Saturation and Development of Necrosis in EMT6/Ro Multicellular Spheroids by the Glucose and Oxygen Supply”. In: *Cancer Research* 46.7 (1986), pp. 3504–3512.

[33] Hlatky L. and Alpen E. L. “Two-dimensional diffusion limited system for cell growth”. In: *Cell Tissue Kinetics* 18.6 (1985), pp. 597–611.

[34] Terranova V. P., DiFlorio R., Lyall R. M., Hic S., Friesel R., and Maciag T. “Human endothelial cells are chemotactic to endothelial cell growth factor and heparin”. In: *J. Cell Biol.* 101.6 (1985), pp. 2330–2334.

[35] Greenspan H. P. “On the growth and stability of cell cultures and solid tumors”. In: *Journal of Theoretical Biology* 56.1 (1976), pp. 229–242.

[36] Greenspan H. P. “Models for the growth of a solid tumor by diffusion”. In: *Stud. Appl. Math* 51.4 (1972), pp. 317–340.

[37] Keller E. F. and Segel L. A. “Model for chemotaxis”. In: *J. Theor. Biol.* 30.2 (1971), pp. 225–234.

[38] Carter S. B. “Principles of cell motility: the direction of cell movement and cancer invasion”. In: *Nature* 208.5016 (1965), pp. 1183–1187.